Geoscience Frontiers 16 (2025) 101953

Contents lists available at ScienceDirect

Geoscience Frontiers

journal homepage: www.elsevier.com/locate/gsf

Research Paper

Combined study of Au-bearing arsenopyrite of orogenic gold deposits (NE Asia): High resolution 3D X-ray computed tomography, LA-ICP-MS, and EMPA data

Evgeny Naumov [a], Yuri Kalinin [b], Galina Palyanova [b,*], Lyudmila Kryuchkova [c], Viacheslav Voitenko [d], Vera Abramova [e], Franco Pirajno [f]

[a] Central Research Institute of Geological Prospecting for Base and Precious Metals, Moscow, Russian Federation
[b] Sobolev Institute of Geology and Mineralogy, Siberian Branch of Russian Academy of Sciences, Novosibirsk, Russian Federation
[c] St. Petersburg State University, SPbSU, St. Petersburg, Russian Federation
[d] Geological Center of SPbSU, St. Petersburg, Russian Federation
[e] Institute of Geology of Ore Deposits, Petrography, Mineralogy and Geochemistry, Russian Academy of Sciences, Moscow, Russian Federation
[f] University of Western Australia, Centre of Exploration Targeting, Australia

ARTICLE INFO

Article history:
Received 13 March 2024
Revised 7 August 2024
Accepted 12 October 2024
Available online 18 October 2024
Handling Editor: C. Manikyamba

Keywords:
High resolution 3D X-ray
Computed Tomograph
Gold-bearing arsenopyrite
Suzdal at East Kazakhstan
Olympiada and Bazovskoe (Russia)
Orogenic gold deposits

ABSTRACT

The distribution of gold in small acicular arsenopyrite of a pyrite-arsenopyrite association from Suzdal (Eastern Kazakhstan), Olympiada (Yenisei Ridge, Russia) and large pseudorhombic arsenopyrite crystals from Bazovskoe (Yakutia, Russia) orogenic-type deposits were investigated. On orogenic gold deposits in NE Asia, occurring mainly in black shales, two productive stages of ore deposition are distinguished, which correspond to two morphological varieties of arsenopyrite. At the early stage, fine-grained acicular-prismatic arsenopyrite with invisible gold was deposited; at the late stage, tabular arsenopyrite in association with free visible gold was formed. The samples of gold-bearing arsenopyrite were analyzed using Scanning Electron Microscopy, Electron Microprobe Analyses, Atomic Absorption and Laser Ablation Inductively Coupled Plasma Mass Spectrometry in combination with High Resolution 3D X-ray Computed Tomography (HRXCT). HRXCT does not destroy the studied mineral during the investigation. That technique permits to do an estimation of the amount of gold inclusions in minerals or host rocks and draw reasonable conclusions about the gold content of the ores, to study in detail the distribution patterns of metal inclusions (associated with certain minerals, cracks, crystal growth faces, etc.) and to determine the form of the gold. It can be used to understanding of the genesis of productive mineral associations, and to developing optimal technological schemes for gold extraction.

1. Introduction

Gold has historically been a key strategic economic commodity. Orogenic gold deposits (as defined by Groves et al., 1998) dominantly form in metamorphic rocks in the mid- to shallow crust (5–15 km depth), at or above the brittle-ductile transition, in compressional settings that facilitate transfer of hot gold-bearing fluids from deeper levels (Goldfarb et al., 2005; Phillips and Powell, 2010; Goldfarb and Pitcairn, 2023). The term "orogenic" is used because these deposits likely form in accretionary and collisional orogens (Groves et al., 1998). Orogenic gold deposits provide more than 75% of gold recovered through human history (Phillips, 2013), and remains most productive and perspective type of gold deposits in the world.

Gold, in most gold deposits with a disseminated mineralization is associated with sulphides, usually arsenopyrite (orogenic deposits in black shale) or arsenic-bearing pyrite (Carlin-type deposits, etc.) (Palenik et al., 2004; Deditius et al., 2014). A large number of research work has been devoted to the study of so-called "invisible" gold (not detectable by traditional optical microscopy methods) in sulphides (e. g. Hough et al., 2011; Cook et al., 2013; Tauson et al., 2019; Vikentyev et al., 2021). It is essential to identify the configuration of gold, to establish the timing and relationship between gold and sulphides, and to develop methods and technological schemes for the extraction of gold from the "resistant" ores. However, many questions remain debatable (Cathelineau et al.,

* Corresponding author at: Novosibirsk State University, Novosibirsk, Russian Federation.
E-mail address: palyan@igm.nsc.ru (G. Palyanova).

https://doi.org/10.1016/j.gsf.2024.101953

1989; Benzaazoua et al., 2007; Sung et al., 2009; Trigub et al., 2017). For example, whether gold in sulphides is isomorphic or structurally bound with the formation of stable and metastable phases in the form of nanoparticles or does it occur as clusters of mono- or multi-element composition. Does co-crystallization of gold and sulphides happen simultaneously, or is there a later deposition of gold on sulphide crystal margins because of adsorption or electrochemical processes? The HRXCT method can help to take a new look at some of these questions (Naumov et al., 2019).

The paper presents the results of studies of gold-bearing arsenopyrite from three typical orogenic gold deposits in NE Asia such as Suzdal (East Kazakhstan), Olympiada (Yenisei Ridge, Russia) and Bazovskoe (Yakutia, Russia). The samples of gold-bearing arsenopyrite were analyzed using traditional methods of a material research (Scanning Electron Microscopy with energy-dispersive X-ray spectroscopy (SEM/EDS), Electron Microprobe Analyses (EMPA), atomic absorption (AAS) and Laser Ablation Inductively Coupled Plasma Mass Spectrometry (LA-ICP-MS)) in combination with High Resolution 3D X-ray Computed Tomography (HRXCT). The HRXCT method gives a three-dimensional image of the phase distribution that differ in density and gives an opportunity to take a new look at controversial issues, such as the forms of gold in sulphides, the thermodynamic characteristics and the time frame of its formation (Cabri et al., 2000; Barnes et al., 2008; Godel, 2013; Kyle and Ketcham, 2015; Fatima et al., 2019; Chisambi et al., 2020; Warlo et al., 2021; da Costa et al., 2022; Lohmeier et al., 2023).

There are several review papers summarizing the available data on the use of HRXCT in general. Cnudde and Boone (2013) presented a review of the principle, the advantages and limitations of X-ray CT itself are indicated, together with an overview of some current applications of micro-CT in geosciences (such as 3D pore, grain, fracture and ore analyses, structural dynamic monitoring, fluid flow and fossils morphological analyses). Kyle et al. (2008) summarize CT principles and review available instrumentation, as well as scanning and data reduction protocols that provide unique three-dimensional information for textural, structural, petrological and fluid inclusion studies for diverse deposit types. Guntoro et al. (2019) study provides a comprehensive overview on the available and potentially useful data analysis methods for processing 3D datasets acquired with laboratory CT systems. These authors indicate that there is a rapid development of new techniques and algorithms capable of processing CT datasets, but application of such techniques is often sample-specific. Several methods that have been successfully implemented for other similar materials (soils, aggregates, rocks) were also found to have the potential to be applied in mineral characterization. The main challenge in establishing a CT system as a mineral characterization tool lies in the computational expenses of processing the large 3D dataset.

Our study differs from many works on 3D X-ray Computed Tomography because it was prepared mainly by geologists but with the deep involvement of technical experts who service HRXCT, SEM/EDS, EMPA, AAS, and LA-ICP-MS instruments and who are well aware of the physical principles of its operation and research capabilities of this equipment. The article is to demonstrate the possibilities of using High Resolution 3D X-ray Computed Tomography (HRXCT) to solve a number of specific geological and mineralogical problems. Despite the fact that the HRXCT technique has been around for quite some time, its role in geological and mineralogical studies performed by geologists is still insignificant because of the impossibility of determining the composition of studying minerals (what is necessary for understanding of ore-forming processes). Our work offers an innovative approach consisting in using several research techniques for studying the same samples. Thus, HRXCT allows revealing the internal phase composition of the sample and detecting all mineral dense phases present in the sample. Then, studies of the composition and trace elements using SEM EDS, EMPA AAS, and LA-ICP-MS allow us to accurately identify the studied mineral phases and draw some conclusions about their formation conditions and the genesis of mineralization.

Our study and the cited papers allows to conclude that the HRXCT method have main limitations, and the discretization effects and possible imaging artefacts. However, the method has undoubted advantages, the principal of which is the preservation of the material under study, as well as the possibility of studying morphology, volume of the studied phases and quantitative three-dimensional textural information.

2. Geology and gold mineralization of the Suzdal, Olympiada and Bazovskoe deposits

The location of three gold deposits – Suzdal (Eastern Kazakhstan), Olympiada (Yenisei Ridge, Russia) and Bazovskoe (Yakutia, Russia) is shown in Fig. 1. Characteristics of these orogenic deposits in black shale and information on gold mineralization are given in Table 1.

The Suzdal orogenic gold deposit is situated in the northwestern part of the West Kalba gold belt in Eastern Kazakhstan and belongs to the type of stringer–disseminated mineralized zones hosted in the Lower Carboniferous black-shale volcanic–carbo nate–terrigenous sequences. Mineralization is controlled by the NE-trending Suzdal Fault. In the north, the deposit borders on the Early Triassic Semeytau volcanic–plutonic structure. Mineralization is superposed on the Late Paleozoic complex of metadolerite and quartz porphyry dikes. Ore deposition was a long-term process comprising four stages. The first stage was related to deposition of slightly auriferous pyrite syngenetic to host rocks. The second stage is characterized by formation of the first productive (with invisible gold) fine acicular arsenopyrite mineralization accompanied by sericitization and localized in the tectonic zone. The stockwork ore with pocket–disseminated base metal mineralization and free microscopic native gold of the third stage is hosted in silicified rocks. The ore formation has been completed by quartz–stibnite veins superposed on all preceding types of mineralization. The geology and mineralogy of the ores of the Suzdal deposit are described in detail in our previous publications (Kovalev et al., 2009, 2011, 2012; Rafailovich, 2009; Kalinin et al., 2019).

The world-class Olympiada orogenic gold deposit is located within the Eastern gold belt in the Neoproterozoic orogen of the Yenisei Ridge at the western margin of the Siberian craton (Krasnoyarsk region, Russia). Its reserves are estimated about 1000 t of Au, and ore mineralization has been traced to depths of more than 1500 m. This deposit is controlled by a large scale and long-lived Tatar-Ishimbinski tectonic zone in deformed Neoproterozoic carbonate-clastic rocks. As a whole, the Olympiada deposit is characterized by a unique composition of ores, the complexity of the geological structure and a long multi-stage formation process. The combination of lithological and structural factors was critical for localization of gold mineralization in calcic and siliceous alteration accompanied by early arsenic and late antimony sulphides. As a result, gold associates with diverse sulphides, especially arsenopyrite which were formed in different stages. The geology, ores and characteristics of gold-bearing arsenopyrite of the Olympiada deposit were most fully studied in the recent works of Sazonov et al. (2019b, 2020), Silyanov et al. (2022) and other.

The Bazovskoe orogenic gold deposit is part of the Elga ore cluster of the Adycha-Taryn group of the Yana-Kolyma gold-bearing belt in Sakha (Yakutia) Republic of Russian Federation.

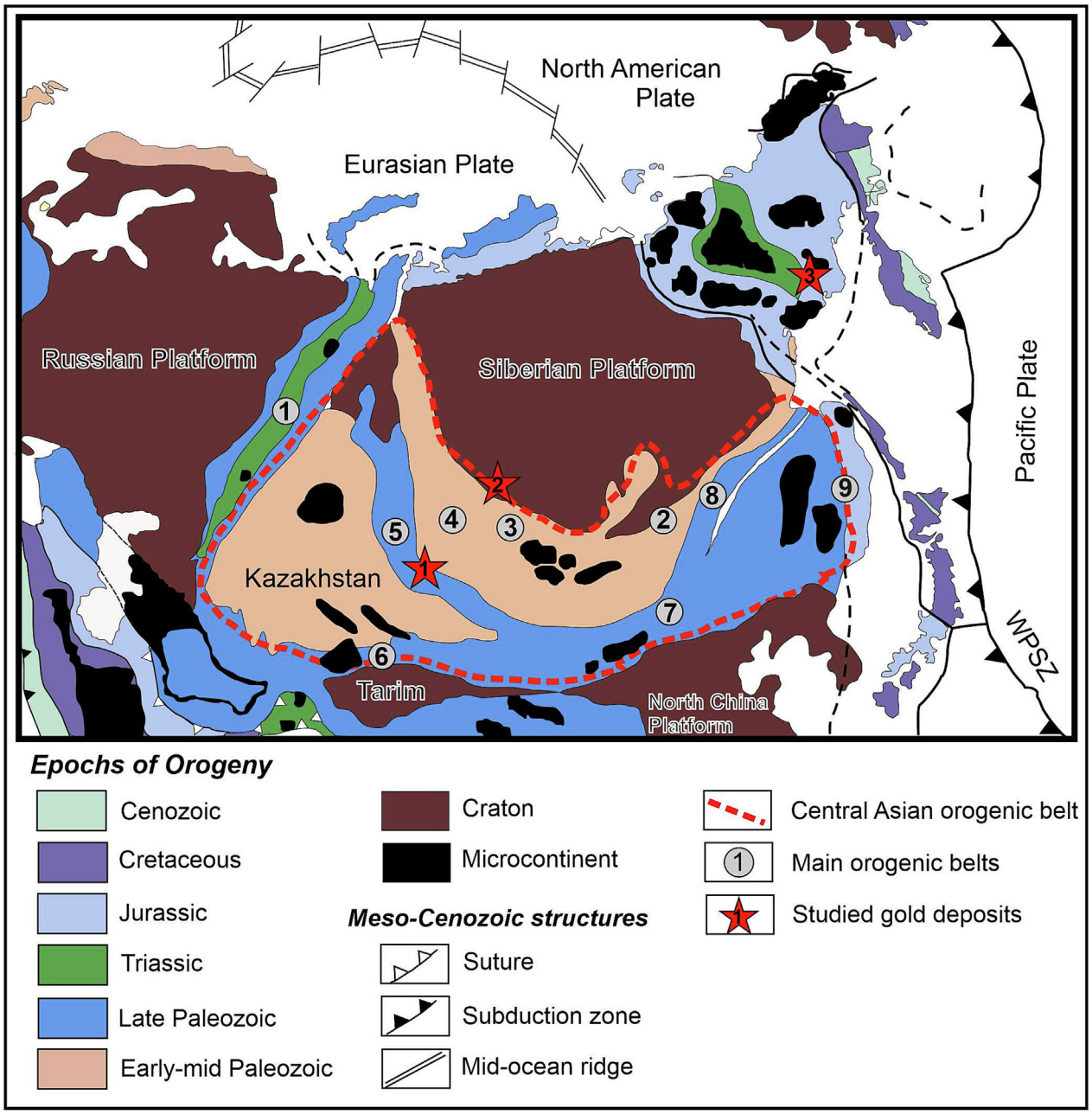

Fig. 1. Tectonic outline of Asia showing major continental blocks surrounding the Central Asian orogenic belt (CAOB), its surroundings and major constituents: orogenic belts and microcontinents (modified after Safonova et al., 2017). Numbers in circles are for orogenic belts: 1 – Uralian; 2–6 Central Asian; 2 – Baikal–Muya, 3 – Yenisey–Transbaikalia–North Mongolia, 4 – Altay–Sayan–NW Mongolia, 5 – Irtysh–Zaisan, 6 – Tienshan; 7 – South Inner Mongolia; 8 – Mongol–Okhotsk; 9 – Sikhote–Alin. Location of studied gold deposits (red star symbol): 1 – Suzdal, 2 – Olympiada, 3 – Bazovskoe. (For interpretation of the references to colour in this figure legend, the reader is referred to the web version of this article.)

The deposit was formed during Late Jurassic-Early Cretaceous accretion-collision processes on the eastern margin of the Siberian craton. The host rocks of the Bazovskoe deposit are the Noriya deposits of the Chernyai formation composed of interbedded predominantly fine- and medium-grained sandstones, sandy siltstones and siltstones. Igneous rocks are represented by rare dikes of Late Jurassic diorite-porphyrites of near-latitudinal strike of the Nera-Bokhapcha complex. Veins in the ore zones of the Bazovskoe deposit are 95%–98% composed of quartz, ore minerals compose 1%–5% and rarely higher. More than 90% of the entire ore mineralization of the deposit is arsenopyrite, which forms metasomatic aggregates ranging in size from 1–7 mm to 10 cm. In cataclastic carbonate-quartz veins and in altered arsenopyrite aggregates, native gold disseminated with sizes ranging from several microns to 0.5 mm is observed. The geological position of the Bazovskoe deposit and the mineralogical and geochemical features of its ores are described in detail in the papers by Fridovsky et al. (2015, 2017, 2023).

3. Materials for research and investigation methods

The distribution of gold in acicular arsenopyrite of a pyrite-arsenopyrite association from Suzdal (Eastern Kazakhstan), Olympiada (Yenisei Ridge, Russia) and large pseudorhombic arsenopyrite crystals from Bazovskoe (Yakutia, Russia) orogenic-type

Table 1
Characteristics of studied gold deposits.

Deposit, region	Suzdal (Eastern Kazakhstan)	Olympiada (Yenisei Ridge, Russia)	Bazovskoe (Yakutia, Russia)
Host rocks	Black-shale volcanic–carbonate–terrigenous sequences (C_1)	Bimica quartz-carbonate sedimentary-metamorphic rocks (NP)	Terrigenous sedimentary rocks (T_3)
Geochemical type	Au-As	Au-As-Sb (Ag, W)	Au-As (Cu, Pb, Zn)
Ore bodies	Vein-disseminated zones; stockwork	Vein-disseminated zones; stockwork	Mineralized zones of crushing, brecciation and mylonitization, silicification
Metasomaic alterations	Silicification, sericitisation	Calcium-siliceous metasomatites	Sericite-ankerite-quartz, chlorite-quartz and albite-chlorite-quartz
Stages of mineral formations (mineral assemblage)	I productive (with invisible gold and fine acicular arsenopyrite) → stockwork ore (tabular arsenopyrite, polysulphides and free microscopic native gold) → Quartz–stibnite veins	Early disseminated Au-As ores (arsenopyrite, pyrite, pyrrhotite, base metal sulfides and native gold). Late disseminated veinlet Au-Sb ores (berthierite, stibnite, native gold, aurostibite, scheelite)	Early (pyrite-arsenopyrite-sericite-quartz metasomatic, pyrite-arsenopyrite-quartz vein), → middle (chalcopyrite-sphalerite-galena) → late (sulfosalt-carbonate)
Quantity and characteristics of samples	12 rock samples, 6 monofractions of arsenopyrite	9 polished sections, 2 monofractions of arsenopyrite	7 polished sections, 1 monofractions of arsenopyrite
Au reserves (C_{Au})	~25 t (6 g/t)	1560 t (4 g/t)	~10 t (13 g/t)
References	Kovalev et al., 2009, 2012	Sazonov et al., 2019a, 2020	Fridovsky et al., 2015, 2017, 2023

deposits were investigated. Details of the sample localities and brief description of the samples are provided in Table 1.

The composition of arsenopyrite and the content of impurities in arsenopyrite were carried out on a JEOL JXA-8100 electron probe micro-analyzer, in the Center for Multiple Element and Isotope Studies of the Siberian Branch of the Russian Academy of Sciences. Monomineral fractions of arsenopyrite were collected under a binocular microscope from crushed and sulphide concentrates, placed in a mounts block and polished. The bulk of arsenopyrite grains was studied at the edges and in the center; in complex star-shaped aggregates – five to eight points. The analytical conditions were as follows: accelerating voltage of 20 kV; beam current of 25 nA; measurement time of 20 s; K series for Fe, Co, Ni, Cu and S; M series for Au and Pb; L series for As and Sb. The standards used were: FeS_2 for Fe and S, FeAsS for As, Fe-Ni-Co alloy for Co, Ni, Au-Ag alloys for Au and Ag, $CuSbS_2$ for Sb, and PbS for Pb. The detection limit for the unilateral 2σ criterion with a confidence level of 97.5% is 30 ppm. The detection limits of other elements in arsenopyrite (wt.%) are: Fe – 0.018, As – 0.06, S – 0.02, Sb – 0.04, Ni – 0.005, Co – 0.004, Zn – 0.043, Cu – 0.02, for Ag (ppm) – 470.

The content of noble metals (Au and Ag, Table 2) in carbonaceous rocks with disseminated pyrite-arsenopyrite mineralization from Suzdal deposit was determined by an atomic absorption method (AAS) using Perkin-Elmer 503 spectrometer with an electrothermal HGA-74 atomizer and a deuterium background corrector, a 3030 system with an HGA-600 atomizer. The detection limit of Au is 0.5 μg/L, Ag is 1 μg/L.

The chemical composition of the arsenopyrite samples of the Olympiada deposit was studied by inductively coupled plasma mass spectrometry (ICP-MS) and laser ablation (LA), the Thermo XSeries 2 quadrupole mass spectrometer equipped with New Wave Research UP-213 laser. Laser parameters: Nd — YAG, radiation wavelength 213 nm, beam energy (fluence) 4.5–6.5 J/cm^2, pulse repetition rate 15 Hz, ablation spot diameter 40–60 μm, carrier gas He, a flow rate of 0.65 L/min; with ablation by a profile, a speed of 7 μm/s. Analysis time: 30 s (background, idle) + analysis time (in the case of a point 60 s, profile – length/speed) + 30 s (flushing). Mass spectrometer parameters: RF Power – 1250 W, working gas – Ar, carrier flow rate 0.95 L/min, plasma-forming flow Ar – 15 L/min, cooling flow Ar – 0.9 L/min. The mass spectrometer was calibrated using multi-element calibration solutions. For calibration and calculation, international standards were used: USGS MASS-1 sulphide and UQAC-FeS1 (UQAC, Chicoutimi, Canada) pressed trace mineral powder doped with natural sulfide. The calculation was carried out with the Iolite software using ^{57}Fe (or ^{33}S) as an internal standard. LA-ICP-MS analyses were carried out at the IGEM RAS by V. Abramova.

Nineteen samples with arsenopyrite were scanned at the Center of X-ray Diffraction Studies of Saint Petersburg State University, Saint Petersburg, Russia, using a SkyScan Bruker 1172 MicroCT scanner and a SkyScan Bruker 2011 NanoCT scanner. Three large

Table 2
Gold and silver content (AAS data) in carbonaceous rocks with disseminated pyrite-arsenopyrite mineralization, Suzdal deposit.

Sample	Rock description	Rock sample		Monomineral sample (arsenopyrite)	
		Au (ppm)	Ag (ppm)	Au (ppm)	Ag (ppm)
Su-20x	Interbedded siltstone and sandstone	3.43	0.47		
Su-21	ditto	3.6	0.4		
Su-21x	ditto	1.71	0.25		
Su-23	ditto	31.0	0.32		
Su-23a	ditto	41.1	0.17		
Su-24	Sandstone	32.2	0.14	830.0	4.0
Su-25	ditto	8.1	0.22		
Su-27	ditto	10.6	0.09	297.0	3.4
Su-29	ditto	26.9	0.26		
Su-30	Brecciated sandstone	8.1	0.77		
Su-40	ditto	13.0	0.33		
Su-63	carbonaceous siltstone	42.0	0.42	288.0	3.2
Sz-18	Tabular arsenopyrite			7.4	0.92
Su-81	Tabular arsenopyrite			2.0	4.6
D-1	Tabular arsenopyrite			88.0	9.1

samples were scanned by means of a SkyScan Bruker 1172 scanner. The three-dimensional mCT datasets were acquired with an acceleration voltage of 100 kV, an e-beam current of 100 μA (Cu radiation, 0.5 mm Al filter and 40 μm Cu filter), exposure 1.7 s, image rotation angle 0.15°, 0.25° and 0.25°, and a resolution of 1.24, 3.59 and 3.59 μm correspondingly. The specimens were scanned using a three-slice mode. The final slices were combined during a single rotation using a NRecon software package (BruckerMicroCT), since it is a capable of neutralizing the instrumental artefacts and can provide a gray scale diapason corresponding to X-ray absorption, and, consequently, to chemical composition of the sample. A total of 1146, 6658, and 4558 individual transverse slices with a matrix size of 2000 × 2000, 4000 × 4000, and 4000 × 4000 were exported into 16 bit TIFF image stacks.

Sixteen small crystals of arsenopyrite were scanned by means of a SkyScan Bruker 2011 scanner. The three-dimensional mCT datasets were acquired with an acceleration voltage of 50 kV, an e-beam current of 200 μA (X-ray source: cathode LaB6, target W) 0.5 mm Cu filter, exposure 2 s, image rotation angle 0.2 degree, and a minimal resolution of 250 nm. A resolution depends on a size of sample – the smaller size of a sample the closer the sample can be moved to X-ray source the higher resolution can be obtained. All these samples were scanned using a three-slice mode as well. The final slices were combined during a single rotation using a NRecon software package. A total of 925 individual transverse slices with a matrix size of 1280 × 1280 were exported into 16 bit TIFF image stacks.

Post-processing of the two-dimensional still images and three-dimensional digital reconstructions were performed using DataViewer and CTVox (BrukerMicroCT) software packages.

4. Results

4.1. The morphological types of gold-bearing arsenopyrite

Generally, two morphological types of arsenopyrite, acicular-prismatic and coarse-crystalline, are characteristic of the gold-sulphide orogenic deposits. At the Suzdal gold deposit (Eastern Kazakhstan) which is well studied by a number of researchers (Kovalev et al., 2009, 2012; Rafailovich, 2009; Kalinin et al., 2019) two morphological types of arsenopyrite are present: acicular and tabular. Acicular arsenopyrite is the main gold-bearing mineral at Suzdal and at many other orogenic gold deposits (Kovalev et al., 2011; Kalinin et al., 2015; Naumov et al., 2015; Sazonov et al., 2016, 2019a, 2019b; Fridovsky et al., 2023). Acicular crystal aggregates have been studied using HRXCT. Such arsenopyrite found in disseminated ores of the early pyrite-arsenopyrite productive association. It is represented by small crystals and its aggregates ranging in size from few to hundreds micron, forming star-shaped and druse-like accretions of acicular and prismatic crystals (Figs. 2 and 3) in metamorphosed carbonaceous siltstones and sandstones.

Mineralized carbonaceous terrigenous rocks contain gold up to tens of ppm (Table 2). The degree of gold content is proportional to the saturation of finely dispersed sulphides, mainly arsenopyrite. In Fig. 2 a photomicrograph of a polished section (right photo) of typical gold-bearing ore of the Suzdal deposit, and HRXCT 3D image (left photo) of microcore (d = 5 mm) of the same rock, with disseminated arsenopyrite are illustrated. Arsenopyrite grains have elongated or isometric pseudohexagonal shape. They contain inclusions of suphides, native gold and other minerals.

It is assumed that the deposition of micro-grains and nano particles of gold in arsenopyrite crystals occurs synchronously with crystal growth. With rapid growth, gold is distributed relatively evenly in the structure of arsenopyrite, with slow growth gold clusters are formed (Fougerouse et al., 2016), and when crystal growth stopped, large visible dendritic crystals or films of gold precipitate along the faces of the arsenopyrite crystals (Voitenko, 2014). Arsenopyrite of the Suzdal deposit (Fig. 3) is characterized by submicron grains of gold, which are extremely unevenly distributed (Fig. 3B).

Tabular arsenopyrite is most widely represented in the Suzdal deposit in late gold-polysulphide association. It is distinguished by flattened isometric crystals, often of a rhombo-pyramidal shape or their druse-like intertwine hosted in silicified and mineralized metasomatic brecciated rocks and in a mineralized dyke of quartz porphyry. Twin crystal intergrowths are usual. Arsenopyrite grains have elongated or isometric pseudohexagonal shapes. They contain inclusions of ore and non-metallic minerals and have a poikilitic structure. Submicroscopic inclusions of gold are found within the arsenopyrite grains. Commonly, gold grows on surface of crystals of tabular arsenopyrite. The association of tabular arsenopyrite with pyrite of the pentagon-dodecahedral shape containing inclusions of visible gold is usual. Tabular arsenopyrite was described in details (Kovalev et al., 2009, 2011). These papers contain micrographs of tabular arsenopyrite.

Main Au-bearing mineral of the Olympiada gold deposit is arsenopyrite, which is subdivided into 2 main associations according to time of formation, morphology and composition: acicular aggregates of earlier arsenopyrite-1 enriched by S; and late coarse-crystalline arsenopyrite-2 enriched in As (Fig. 4, Table 3). These types represent distinct ore forming events and differ by Au contents. First type is characterized by elevated contents of Au averaging 330 ppm, whereas arsenopyrite 2 contains only about 30 ppm of Au.

Arsenopyrite also prevails in the ore assemblages of the Bazovskoe deposit. Early arsenopyrite is metasomatic, disseminated in the near-ore rocks, often associated with pyrite. Late arsenopyrite usually forms metacrystals 1–7 mm in size in quartz veins, less commonly forms clusters up to 10–30 cm in size. Arsenopyrite often replaces by scorodite (Fig. 7).

4.2. The composition of arsenopyrite

The average chemical composition of needle-prismatic and tabular arsenopyrite of the Suzdal and the Olympiada deposits and large pseudorhombic arsenopyrite crystals from the Bazovskoe deposit is somewhat different; the ratio of sulfur and arsenic in them is shown in the diagram (Fig. 4). The composition of acicular arsenopyrite in the early productive association is non-stoichiometric. The sulphur content is in the range of 21–24 wt. %. S/As ratios in them are 1.16–1.21. Trace elements (according to EMPA), such as Sb, Ni, and Co, were detected. Silver content in monomineralic samples of arsenopyrite of both morphological differences is low, varying within 0.92–9.10 ppm. Other elements were found in an insignificant number of the samples at concentrations close to the detection limit.

The disseminated gold-arsenopyrite mineralization is the main productive stage at the Olympiada orogenic gold deposit located in the Yenisei Ridge (Russia) and described in detail in many papers (Cabri et al., 2000; Nozhkin et al., 2011; Naumov et al., 2015; Sazonov et al., 2019b, 2020; Silyanov et al., 2022 and many other). Disseminated gold-arsenopyrite mineralization is associated with carbonate-aluminosilicate and siliceous rocks and is the main type of gold-bearing ore. Ore-bearing rocks retain the primary layered and rhythmically layered structure with a wide variation of chemical composition, both in microlayers and in larger strata. The layers are represented by calcareous, carbonaceous-calcareous-aluminosilicate, siliceous and carbonaceous-siliceous rocks and contain carbonates, biotite, sericite, chlorite, zoisite, albite, quartz, with accessories of tourmaline, rutile and apatite. The abundance

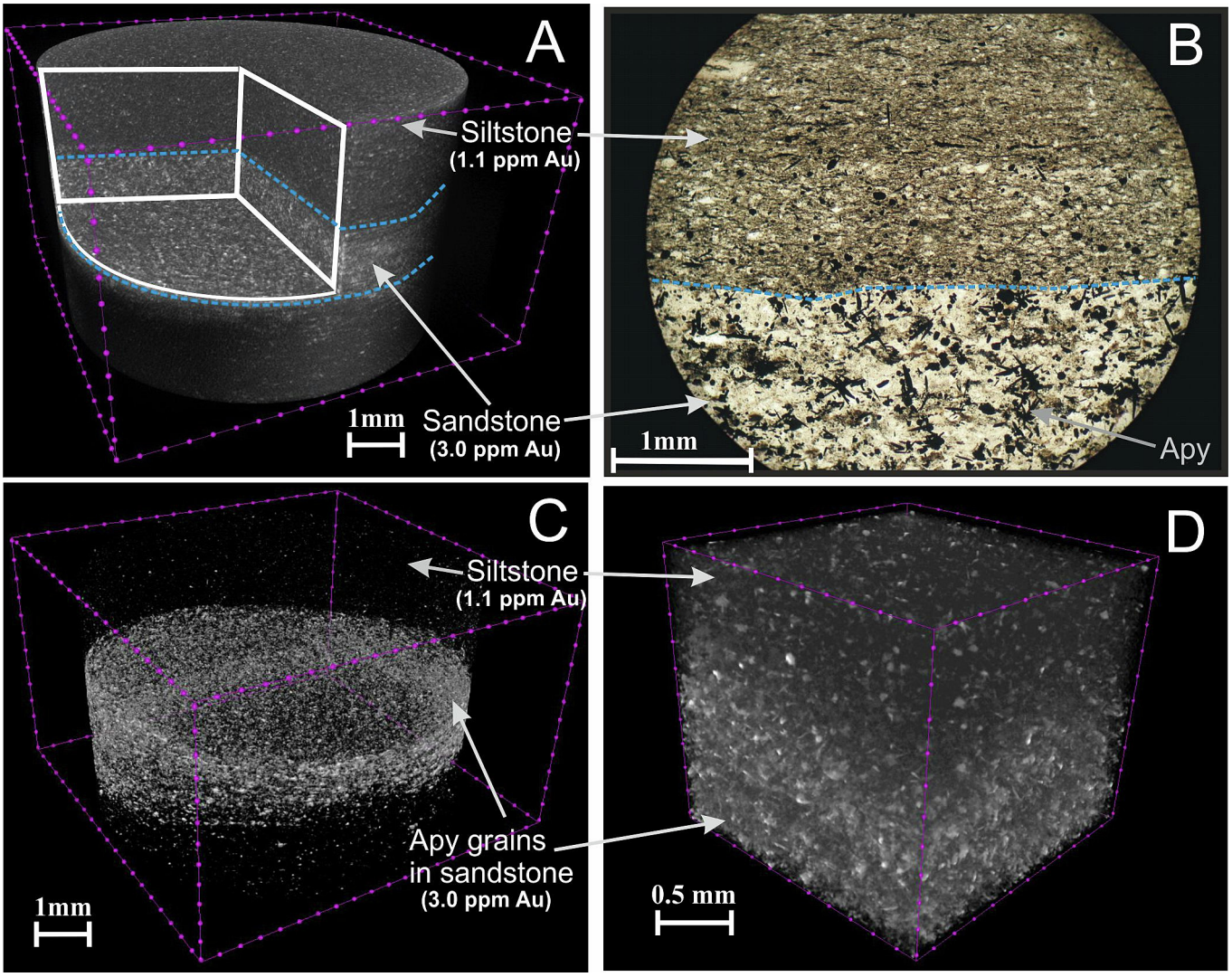

Fig. 2. A layer of sandstone enriched with arsenopyrite (Apy) in siltstone, in the Suzdal deposit, Su-27 microcore sample. (A) HRXCT 3D image (light grains are arsenopyrite); (B) photomicrograph of polished thin section (black grains – arsenopyrite); (C) HRXCT 3D image, aggregates of acicular arsenopyrite; (D) enlarged fragment of arsenopyrite-bearing rock.

of finely interspersed pyrrhotite-arsenopyrite mineralization of these rocks is about 3%–5%, however its distribution in layered varieties is extremely uneven. They are commonly characterized by layered distribution with individual layers depleted or enriched in sulphides. Petrographic study of thin sections gold-bearing arsenopyrite from the Olympiada deposit shows that the acicular arsenopyrite is located in a fine-grained quartz-carbonate-micaceous aggregate, locally interspersed with garnet, biotite and zoisite. The gold content in such samples varies from few to tens of ppm (Sazonov et al., 2020; Silyanov et al., 2022). Arsenopyrite occurs a fine-acicular or fine-prismatic crystals. The size of these crystals varies in length from tens to hundreds of microns (Fig. 5A).

There are both intergrowths of single crystals and stellar aggregates of arsenopyrite, which resemble the arsenopyrite of the Suzdal deposit discussed above. Commonly, the crystals have a skeletal structure and contain inclusions of pyrrhotite. The paragenetic relationship of these minerals is not always unequivocally established.

Fine grains of high grade gold were detected in the acicular arsenopyrite. It can also be determined by HRXCT. The monomineralic fractions of acicular arsenopyrite from the OK-108 sample, analyzed by the atomic absorption method, contain 348 ppm Au and 0.92 ppm Ag. The chemical composition of acicular arsenopyrite, according to EMPA, is given in Table 3. Most analyses of arsenopyrite reveal its non-stoichiometric varieties enriched in sulphur and depleted in arsenic. Ni and Co contents in arsenopyrite is mainly in amounts of up to 0.045 wt.% and 0.14 wt.%, respectively.

LA-ICP-MS trace elements study of the acicular arsenopyrite crystals from Olympiada deposit showed contents of gold close to the AAS and EMPA data. However, the capacities of this method make it possible to determine the trace elements content directly at the analysis point or within the micron length profiles. The analysis results are presented in Table 4. LA-ICP-MS studies showed a uniform distribution of gold within the crystals (Fig. 5), which is clearly displayed in the graphs of Fig. 6. However, in some crystals of arsenopyrite an uneven distribution of antimony was established (Fig. 6b, sample OK-108-29). Moreover, the distribution of antimony does not correlate with the distribution of other elements, and SEM/EDS studies did not show the presence of microinclusions of Sb-containing minerals. This fact needs farther detailed investigation.

Many previous studies (Cathelineau et al., 1989; Benzaazoua et al., 2007; Sung et al., 2009; Kovalchuk et al., 2019; Tauson

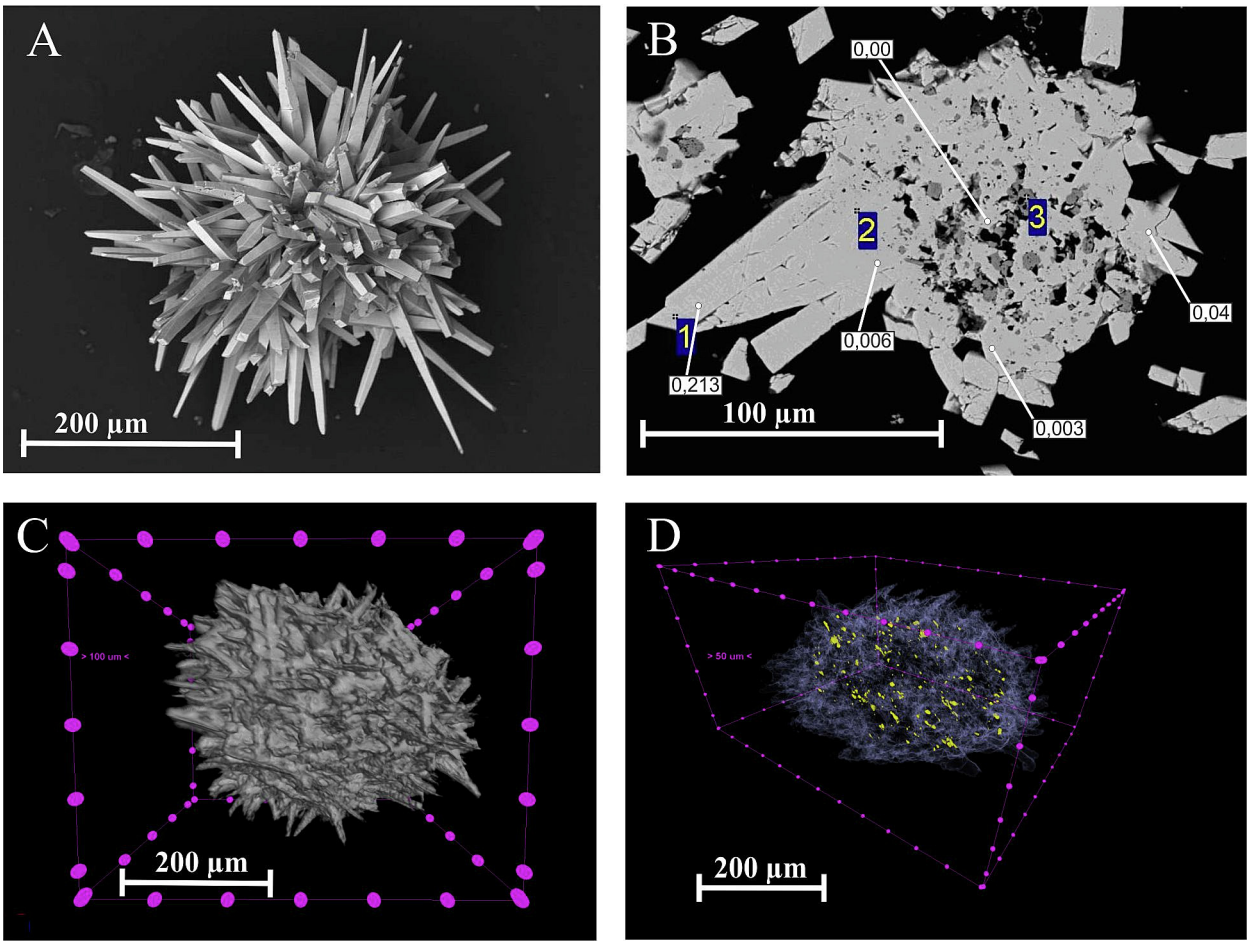

Fig. 3. Aggregates of gold-bearing arsenopyrite crystals (sample Su-27) from the Suzdal deposit (East Kazakhstan). (A) A scanning electron microscope image. (B) BSE image of arsenopyrite with highlighted points of gold content determined by micro X-ray analysis (wt.%). (C and D) HRXCT 3D reconstruction. (C) Opaque appearance of arsenopyrite; (D) arsenopyrite grain is shown in transparent grey contour, the yellow points represent the inclusions of gold. (For interpretation of the references to colour in this figure legend, the reader is referred to the web version of this article.)

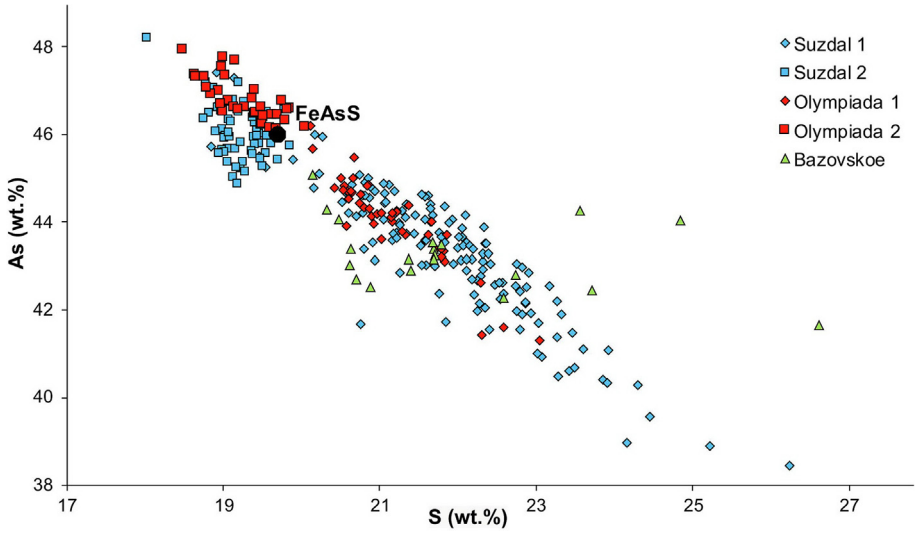

Fig. 4. As–S diagram for morphologic varieties of arsenopyrite in comparison with its standard chemical composition (FeAsS). Suzdal 1, Olympiada 1 – acicular arsenopyrite formed in the early mineralization stage; Suzdal 2, Olympiada 2 – tabular arsenopyrite formed in the late mineralization stage; green triangle – gold-bearing arsenopyrite, Bazovskoe deposit. (For interpretation of the references to colour in this figure legend, the reader is referred to the web version of this article.)

et al., 2019; Vikentyev et al., 2021) assumed that arsenopyrite crystals contain only "invisible" gold as trace isomorphic admixtures in arsenopyrite. HRXCT study confirmed that significant part of the gold form relatively large (1–3 µm) native grains in arsenopyrite samples from Suzdal and Olympiada deposits (Figs. 3D and 5B, 5C). Gold particles are concentrated on the surface of acicular

Table 3
Composition of arsenopyrite in OK-108 sample, Olympiada deposit (in wt.%) (EMPA). Analyses were carried out at the IGM SB RAS, Novosibirsk, Russia.

No	S	As	Ni	Fe	Au	Sb	Co	Total
1	21.02	44.19	0.026	33.60	0	0.23	0.069	99.14
2	20.75	44.43	0.045	33.56	0	0.295	0.087	99.17
3	20.85	44.82	0.016	33.43	0.057	0.23	0.063	99.47
4	21.14	44.10	0.024	33.58	0.047	0.215	0.068	99.19
5	20.57	43.90	0.033	33.73	0.005	1.202	0.063	99.52
6	19.75	46.76	0	33.0	0	0	0.143	100.06

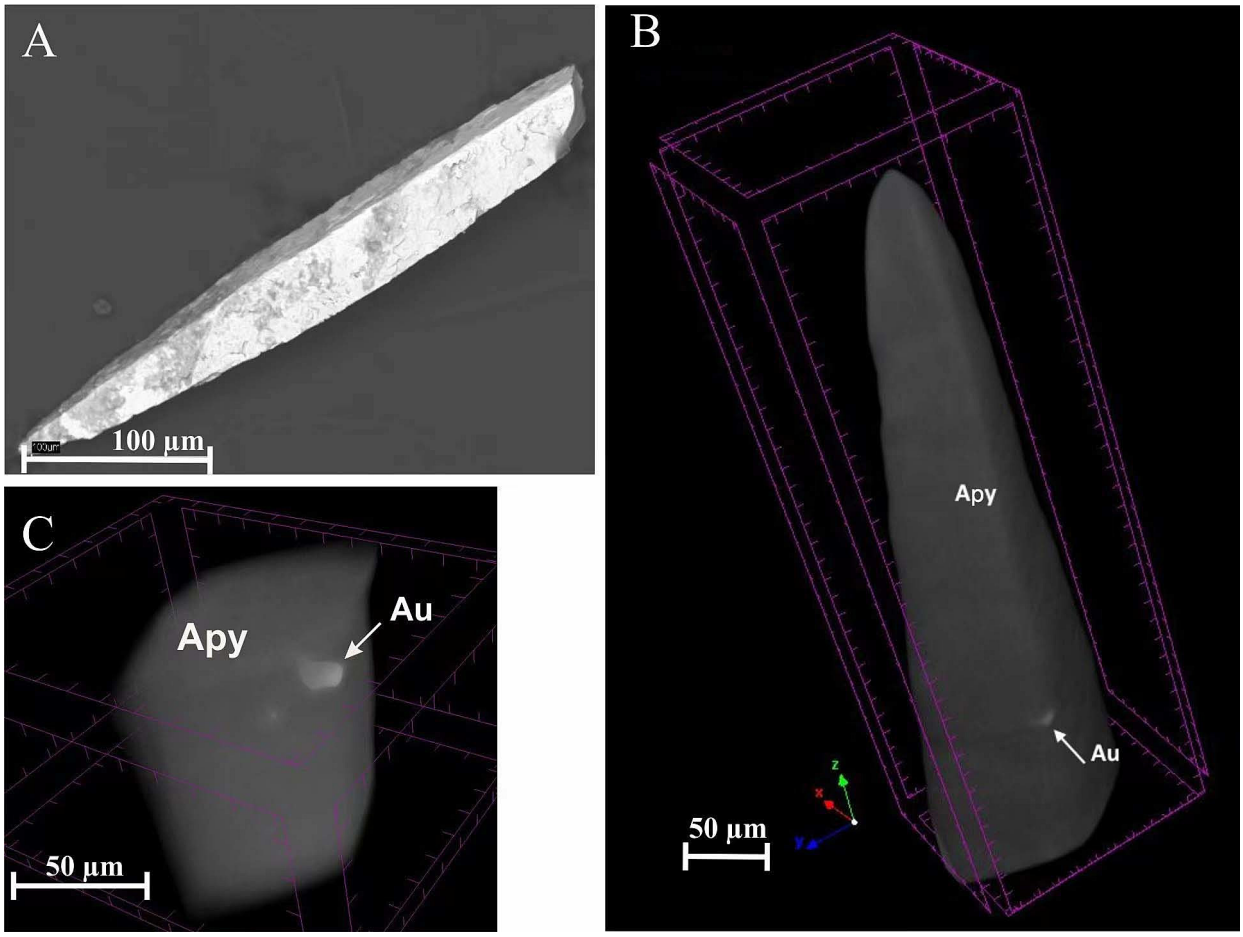

Fig. 5. Acicular microcrystals of gold-bearing arsenopyrite from the Olympiada deposit, sample OK-108. (A) SEM image. (B) HRXCT 3D image. (C) Enlarged 3D fragment of Fig. 3B.

Table 4
Trace impurities in arsenopyrite, OK-108 sample, Olympiada deposit, made by LA-ICP-MS (concentration in ppm).

Point No	Co	Ni	Cu	Zn	Sb	Te	Ba	Au	Pb
OK108-17	277.40	180.50	7695.00	1330.00	61560.00	15.01	2.41	381.90	59.47
OK108-21	302.48	189.81	21.66	37.24	8930.00	5.45	6.18	853.10	16.91
OK108-23	296.40	207.10	17.29	49.97	1064.00	3.61	6.84	893.00	5.45
OK108-24	298.30	199.50	20.33	2.09	1900.00	6.27	0.59	195.70	0.74
OK108-27	275.50	184.30	13.49	10.83	21280.00	2.87	1.31	1185.60	26.60
OK108-29	322.62	201.97	17.48	15.20	7790.00	2.03	1.84	340.10	10.64
OK108-32	362.90	253.65	26.41	82.08	11780.00	3.21	8.17	296.40	17.48
OK108-19	299.06	265.05	4.67	0.87	1835.40	3.15	5.55	609.90	1.46
OK108-28	259.35	236.17	2.68	0.19	1535.20	2.49	4.22	294.88	0.58

microcrystals of arsenopyrite from Olympiada deposit or form a micro-inclusions inside in arsenopyrite grains from Suzdal deposit.

In arsenopyrite grains of the Bazovskoe deposit (samples from Vostochnoe ore body) inclusions of pyrite crystals and dendrite-like gold aggregates, as well as disseminated galena, ilmenite, are revealed. Arsenopyrite is substantially sulphuric, the S/As ratio is 0.96–1.16, an average of 1.06, the $\delta^{34}S$ value varies from −0.86‰ to +2.30‰, which is typical for gold-quartz orogenic deposits of

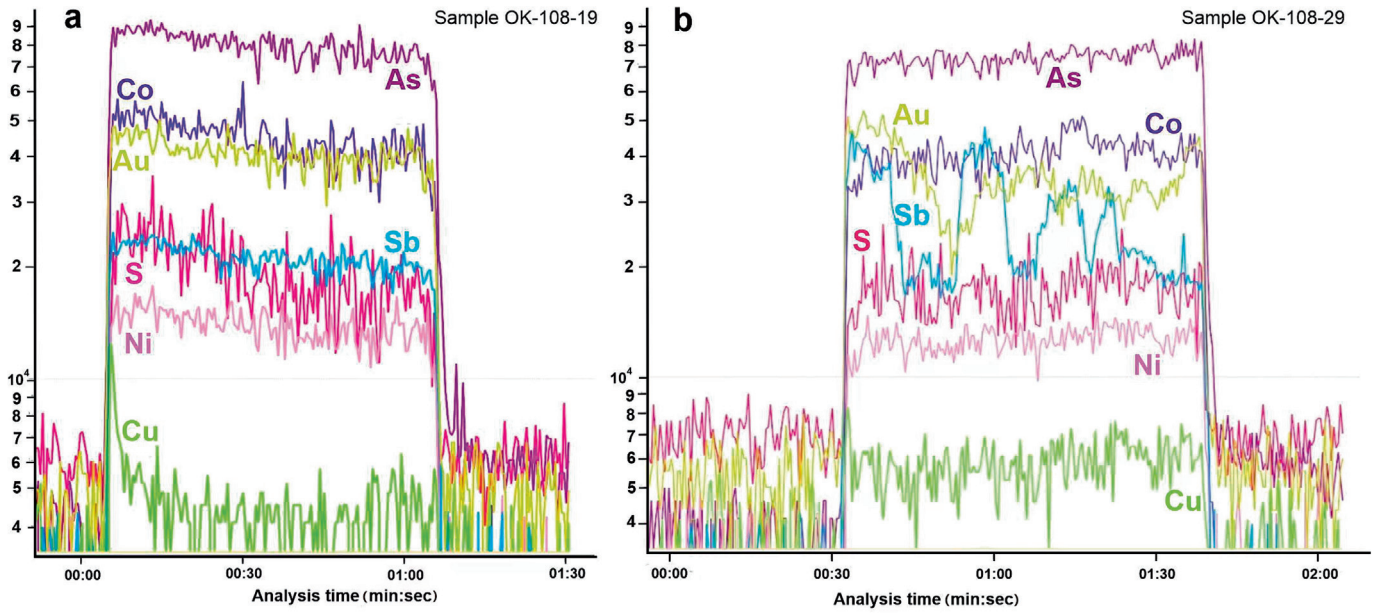

Fig. 6. Representative time-resolved depth profiles for acicular arsenopyrite (from the Olympiada deposit), analyzed in this study indicating the occurrences of gold and other minor and major elements.

the Verkhoyan-Kolyma folded region (Fridovsky et al., 2015, 2017, 2023). The studied arsenopyrite crystals (Table 5) enriched in S, points of arsenopyrite composition are located in the area of gold-bearing arsenopyrite, the same as the arsenopyrite of Olympiada and Suzdal deposits (Fig. 4). Native gold of the Bazovskoe deposit contains a significant admixture of silver (15–16 wt.%), and up to 1.06 wt.% of Hg. Trace amounts of As, Cu, Fe and Sb are also observed in gold grains (Table 6). Studied arsenopyrite represented by metasomatic aggregates from 1–7 mm to 10 cm in size. In carbonate-quartz veins and in modified arsenopyrite aggregates, native gold is disseminated from a few microns to 0.5 mm in size. In polished sections of arsenopyrite ores, gold is represented by parallel elongated aggregates among arsenopyrite single crystals almost completely replaced by scorodite (Fig. 7).

According to HRXCT images, gold in arsenopyrite is represented by elongated crystals, up to 0.2 mm in diameter, forming branched aggregates (Fig. 8). "Coral-like" gold aggregates are located along parallel microcracks within the arsenopyrite crystal, inside which the "branches" form regular intergrowths with each other with dihedral angles of about 51°–54° (Fig. 8B). The angles do not coincide with the angles of the cell of the arsenopyrite crystal lattice (α = 67.6. α = 112.3) and among the characteristic planes of arsenopyrite {0 0 1}, {1 0 1}, {1 1 0}, {2 0 1}, {0 1 1}, {0 1 2}, {0 2 1}, and are suitable only for the dihedral angle formed by the {0 2 1} planes. Thus, gold shows selective crystallization not only within the aggregate of arsenopyrite crystals in the ore zone, but also among the crystallographic directions of a single arsenopyrite crystal. The question remains unanswered whether these crystallographic directions are planes in the areas of tension during deformation of arsenopyrite aggregates or in planes most energetically favorable for gold crystallization (Voitenko, 2014).

Table 5
Composition of arsenopyrite from quartz-sulfides (Apy-Py-Ga) vein of the Bazovskoe deposit (Yakutia, Russia) (EMPA data).

	Sample	wt.%									
		As	Cu	Ni	Co	Fe	Sb	Sn	S	Se	Total
1	B-28/1	45.08	0.00	0.00	0.04	35.00	0.00	0.00	20.15	0.11	100.37
2	803B-140	43.03	0.00	0.03	0.06	33.98	0.00	0.05	20.62	0.16	97.94
3	803B-140	43.37	0.00	0.00	0.06	33.54	0.01	0.00	20.64	0.13	97.75
4	P-5/20	42.53	0.00	0.00	0.04	33.88	0.00	0.01	20.89	0.12	97.46
5	P-5/20	43.37	0.00	0.03	0.09	34.49	0.07	0.02	21.70	0.19	99.96
6	P-5/17	43.26	0.00	0.01	0.06	34.39	0.05	0.02	21.71	0.17	99.66
7	804-122	44.26	0.00	0.02	0.04	33.60	0.01	0.04	23.56	0.14	101.65
8	B-17/2	41.67	0.00	0.00	0.02	33.38	0.04	0.00	26.61	0.15	101.86
9	804-122	43.53	0.00	0.00	0.03	34.17	0.00	0.02	21.69	0.18	99.61
10	P-5/17	43.48	0.01	0.03	0.09	34.24	0.00	0.01	21.80	0.15	99.81
11	804-122	42.80	0.02	0.01	0.06	34.16	0.04	0.03	22.73	0.20	100.05
12	804-122	44.02	0.01	0.00	0.06	33.64	0.06	0.00	24.83	0.11	102.73
13	812-360	44.05	0.04	0.00	0.04	34.13	0.02	0.00	20.49	0.20	98.97
14	812-360	44.28	0.00	0.00	0.00	34.57	0.05	0.01	20.33	0.07	99.30
15	K-805-80	42.45	0.02	0.00	0.01	33.99	0.04	0.00	23.71	0.14	100.36
16	K-640	42.70	0.05	0.07	0.13	34.74	0.05	0.01	20.71	0.14	98.58
17	K-825	42.92	0.00	0.02	0.03	33.83	0.07	0.00	21.40	0.18	98.43
18	K-535	43.15	0.03	0.00	0.09	34.19	0.03	0.01	21.70	0.17	99.36
19	K-825	42.29	0.02	0.00	0.08	33.74	0.04	0.02	22.59	0.02	98.79
20	K-535	43.16	0.07	0.04	0.07	33.77	0.11	0.01	21.38	0.14	98.74

Table 6
Composition of native gold from arsenopyrite of the Bazovskoe deposit (Yakutia, Russia) (EMPA data).

No	Sample	wt.%							
		As	Hg	Au	Cu	Fe	Sb	Ag	Total
1	B-28/1	0.21	0.64	83.90	0.01	0.03	0.00	13.11	97.88
2	B-28/1	0.22	0.53	82.15	0.00	0.00	0.00	13.36	96.27
3	B-28	0.30	1.06	87.29	0.02	0.03	0.00	10.62	99.33
4	B-28	0.27	0.86	84.46	0.00	0.01	0.00	13.22	98.81
5	K-640	0.49	1.01	84.96	0.00	0.04	0.02	10.94	97.47
6	802B-85	0.23	0.43	81.60	0.00	0.02	0.00	15.48	97.78
7	802B-85	0.12	0.87	81.85	0.00	0.00	0.00	15.05	97.90

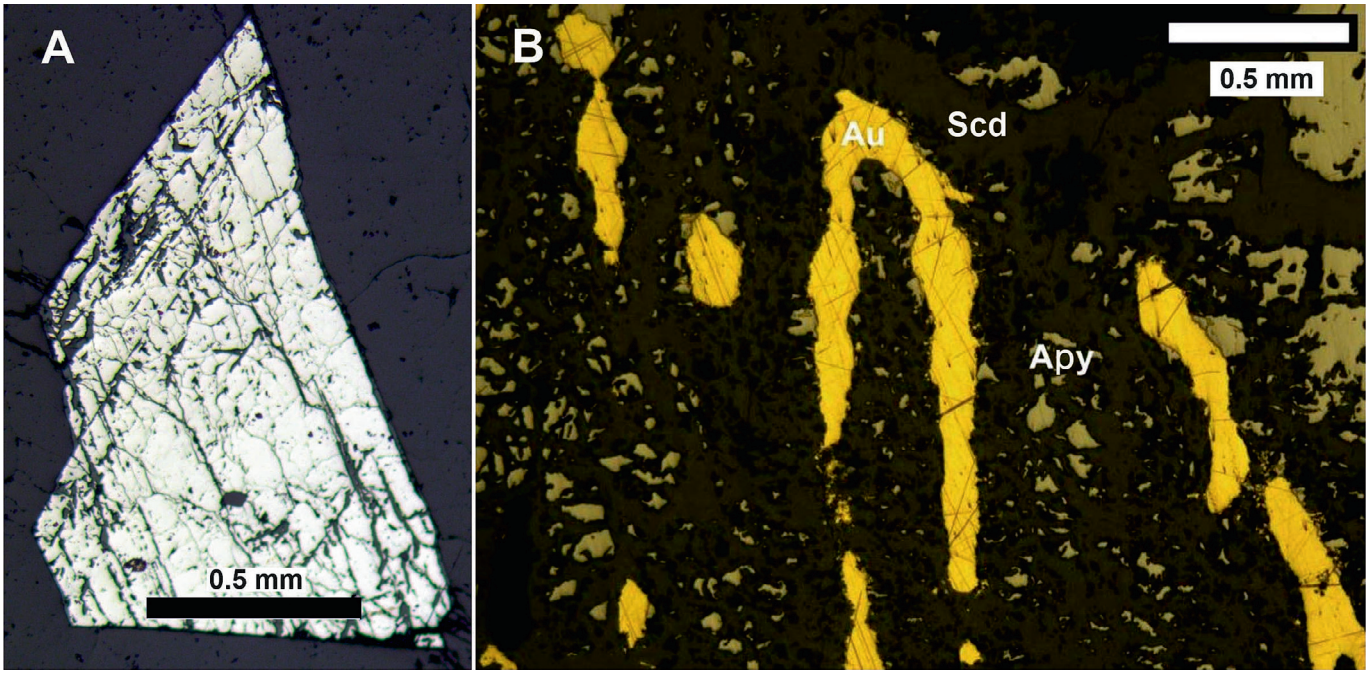

Fig. 7. Arsenopyrite from the Bazovskoe deposit (A) and dendrite-like gold (Au) in arsenopyrite (Apy) replaced by scorodite (Scd) and in plane view of polished section (B). Reflected light.

5. Discussion

Imaging techniques like HRXCT can provide unique information of the geological and metallurgical significance for gold and related ore minerals. This study provides quantitative three-dimensional textural information (e.g., crystal sizes and distributions, degree of interconnectivity, abundances, shapes, textural relationships, intergrowth characteristics, orientation of mineral grains).

Many authors have used computed tomography in the study of ore minerals. For example, Godel (2013) investigated the applicability of HRXCT to Ni-Cu-PGE ore samples from Australian deposits. Kyle et al. (2008) examined the supergiant Grasberg porphyry Cu–Au deposit. Differentiating between metallic mineral grains with relatively small differences in density, e.g., bornite (5.1 g/cm^3) from chalcopyrite (4.2 g/cm^3), is relatively straightforward for isolated monominerallic grains or composites in a similar lower-density matrix, but difficulties are encountered with the interpretation of typical intergrown ore minerals. X-ray beam-hardening artefacts could lead to inconsistency in attenuation determination, both within and among slice images, complicating quantitative processing. However, differentiation of chalcopyrite and bornite was successful in smaller-diameter (b = 22 mm) cores of Grasberg ores. Small-diameter (b = 10 mm) cores of the Grasberg stockwork Cu–Au ore were analyzed and data reduction protocols using the Blob3D software (Ketcham, 2005) were modified to improve the quantification of grain sizes and shapes. Grains as small as 6.5 μm were identified and all of these grains occur in direct contact with chalcopyrite, providing support for gold distribution in porphyry copper systems being a result of exsolution from copper sulphides. Digital radiography combined with micro-CT scanning precisely defined the in situ location of mineral grains of interest within a sample, which then can be studied in conventional petrographic sections, as well as other types of analytical studies (e.g., gold trace element geochemistry). Ghorbani et al. (2011) used a micro-CT scanner for the 3D characterization of crack and mineral dissemination in sphalerite ore particles. In order to distinguish between the different minerals, a dual energy scanning procedure was run to determine both the density and effective atomic number of the minerals of interest. Combination of this information with a prior knowledge of the mineralogical characteristics of the ore, allowed the differentiation of the major minerals of interest in 3D (galena, sphalerite, pyrite and silicate gangue) without the need for laborious sample preparation (such as impregnating, thinning, polishing) and allow the potential applications of X-ray CT to heap leaching technology and future directions. Agorhom et al. (2012) mention that there is a considerable challenge in accurate characterization of gold (Au) particles in low-grade plant ore mineral samples.

Some authors (e.g. Chetty et al., 2012) applied CT methods to the study of gold-bearing ore from the giant Witwatersrand min-

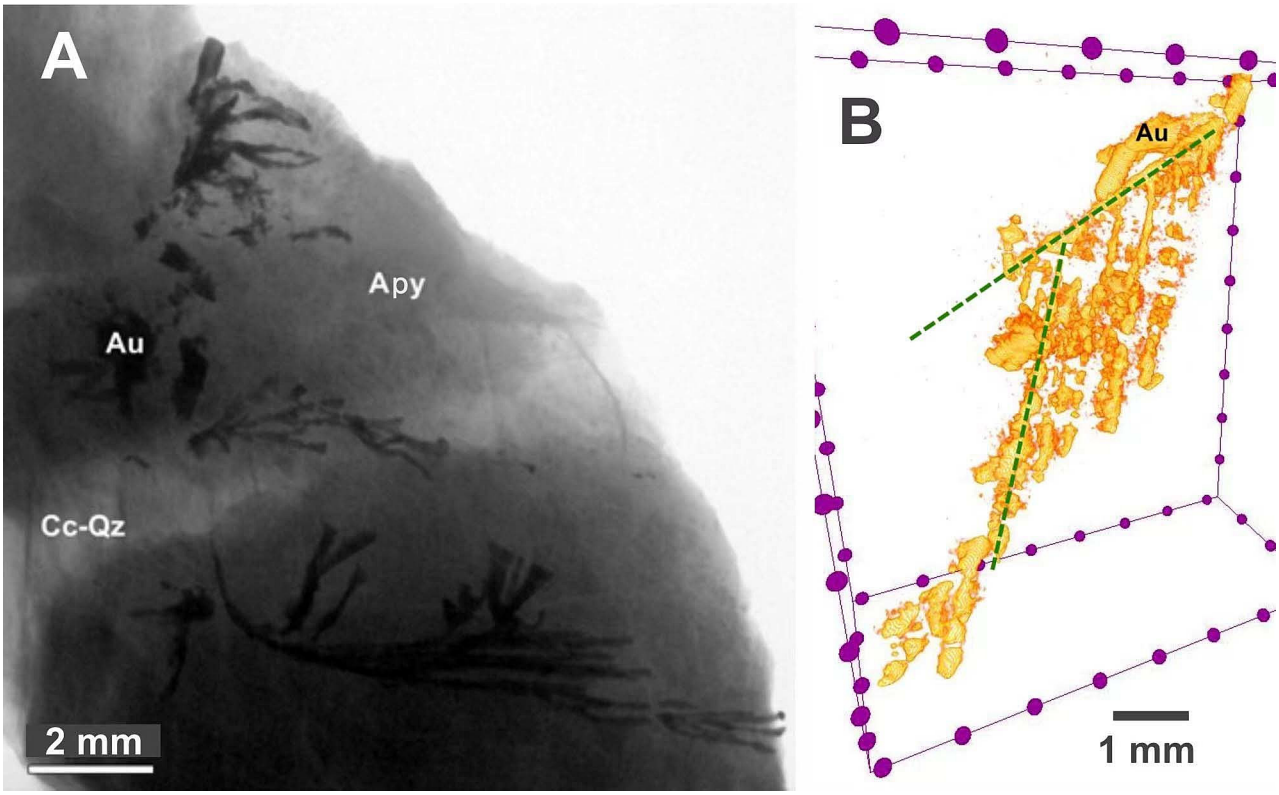

Fig. 8. HRXCT image of dendrite-like gold (Au) in arsenopyrite aggregate (Apy) with calcite-quartz (Cc-Qz) veinlet on raw image (A) and on 3D image (B).

eral field, South Africa. The ability to pinpoint gold occurrence prior to downstream comminution and leaching would potentially reduce processing costs. The aim of the study was therefore to determine to what extent gold, typically fine-grained in occurrence, could be identified in situ. Two gold-bearing drill core slices were investigated using 1-mm focal spot X-ray tomography and micro-focus X-ray tomography (μXCT). Using the derived data, the cores were cut and polished for examination by conventional automated scanning electron microscopy (SEM) to detect gold grains. The SEM results were then compared against the μXCT data. Gold was, to an extent, located by μXCT and validated against SEM data. These first findings suggest that areas rich in gold can be pinpointed by 3DCT prior to conventional assessment, hence potentially reducing processing costs.

Our study, taking in consideration the cited papers, allows us to conclude that the HRXCT method have main limitations such as operator dependency for the 3D image analysis from the reconstructed data, and the discretization effects and possible imaging artefacts. However, the method has undoubted advantages, and can be applied in mineralogy, metallurgy, economic geology and other.

HRXCT study is most effective when it used together with other methods such as optical microscopy, SEM, EMPA, LA-ICP-MS. Many articles have been devoted to the study of the gold-bearing arsenopyrite in orogenic deposits (Arehart et al., 1993; Genkin et al., 1998; Volkov et al., 2007; Kovalev et al., 2011; Bindi et al., 2012; Khishgee and Akasaka, 2015; Trigub et al., 2017; Kovalchuk et al., 2019; Merkulova et al., 2019; Sazonov et al., 2019a, 2019b; Kudrin et al., 2021; Fridovsky et al., 2023), modern studies are usually carried out using LA-ICP-MS (Hinchey et al., 2003; Morey et al., 2008; Cook et al., 2013 and many others). Arsenopyrite from orogenic gold deposits in Siberia was studied by (Genkin et al., 1998; Volkov et al., 2007; Kovalev et al., 2011; Sazonov et al., 2016, 2019b) and others, but most of these papers were published in Russian and are inaccessible to the international geological community.

5.1. The forms of occurrence of gold and its distribution in arsenopyrite

Arsenopyrite is important carrier of Au that is present in the form of microscopic and "invisible" gold. Traditional methods of the analysis made it possible to establish that the content of "invisible" gold in the acicular arsenopyrite of the orogenic deposits (Suzdal and Olympiada) vary within 195–1185 ppm. The gold content in arsenopyrite is quite reliably determined by various methods such as atomic absorption (for bulk arsenopyrite samples), EMPA and LA-ICP-MS for local analyses. Same time in this combined study three-dimensional HRXCT reconstruction revealed micro-inclusions of native gold in the acicular crystals and aggregates of the arsenopyrite of Suzdal and Olympiada deposits, although previously researchers assumed the presence only of "invisible" gold in unspecified form in such acicular crystals.

Apparently, the noble metal is sorbed on the surface of growing crystals, accumulates in structural defects (Tauson et al., 2014; Kravtsova et al., 2015) or forms micro- to nanoscale fills in the microcracks in arsenopyrite (Jelic et al., 2023). Jelic et al. (2023) determined that gold is polycrystalline and consists of nanocrystallites 20–30 nm in size. According to our HRXCT results, gold in arsenopyrite of Bazovskoe deposit forms elongated crystals and branched aggregates (Fig. 8). This "coral-like" gold aggregates shows selective crystallization, which may be related to the structure of arsenopyrite and deformations.

In many deposits, sulfur-rich arsenopyrite contains high concentrations of gold (Cabri et al., 2000; Sidorova et al., 2020; Kudrin et al., 2021 and many others). Our studies confirm that S-enriched arsenopyrite has the highest gold content at low arsenic (Fig. 4), while crystals of this composition are usually have acicular shape and quite small in size. It is assumed that the formation of

such gold-enriched arsenopyrite occurs under conditions of significant supersaturation of hydrothermal solutions with sulfuric-arsenic gold complex, the decomposition of which simultaneously gives rise to a large number of nucleated crystals with a high crystallization rate (Volkov et al., 2007; Kovalev et al., 2011).

Trace elements in arsenopyrite from the Suzdal deposit were studied by EMPA. Among analyzed trace elements (Sb, Ni, Co, Ag, Zn and Cu), the highest concentrations of antimony (up to 1.5 wt. %), nickel (up to 0.5 wt.%) and cobalt (up to 1.0 wt.%) were found in the tabular arsenopyrite. The silver content in monomineral samples of arsenopyrite of both morphological varieties is low, varying between 0.92–9.1 g/t (Table 2). The remaining elements are found in a minor concentrations close to the detection limit.

The arsenopyrite of the Olympiada deposit studied by LA-ICP-MS which determined the contents of such trace components as Co, Ni, Cu, Zn, Sb, Te, Ba, Pb (Table 4) and established a uniform distribution of gold within the analyzed grains (Fig. 6). Also, in some arsenopyrite grains, regular variations in Sb content were revealed (Fig. 6b). This is possibly caused by the zonal structure of arsenopyrite grains. Also Fig. 6b demonstrate that gold sometime distributed unevenly within the arsenopyrite crystals. It can be explained as nanoscale gold clusters (Fougerouse et al., 2016) as any mineral inclusions were not detected with SEM and HRXCT.

5.2. The precipitation mechanism and duration of ore deposition processes

Four possible sources for the fluids and metals forming the orogenic gold deposits have been proposed, such as metamorphic fluids, fluids from the subcrustal area tied to subducted oceanic plates or the fertile mantle, convection of meteoric water, or magmatic-hydrothermal fluids (Groves et al., 2020; Goldfarb and Pitcairn, 2023;). It is widely recognized that fluid cooling, boiling, immiscibility induced by pressure reduction, water–rock interactions, or fluid mixing can lead to gold precipitation (Williams-Jones et al., 2009). Au precipitation can occur if the fluid's H_2S content decreases, oxygen fugacity increases, or changes in pH. Changes in physico-chemical conditions such as temperature, pressure, oxygen fugacity, and sulfur fugacity are effective mechanisms for gold precipitation (Hayashi and Ohmoto, 1991; Jiang et al., 2023; Liang et al., 2023).

The Suzdal, Olimpiada and Bazovskoye deposits differ in the forms of gold in arsenopyrite. According to the obtained EPMA and HRXCT results, 2 forms of gold were revealed for arsenopyrite of the Suzdal deposit – isomorphic (in fine-grained acicular-prismatic arsenopyrite of the early stage), nano and micro inclusions in defects, cracks, on the surface of arsenopyrite crystals (in tabular arsenopyrite of the late stage in association with scorodite). At the early stage of formation of finely disseminated pyrite-arsenopyrite mineralization in sericitized carbonaceous-terrigenous rocks, controlled by tectonic zones. The fluid was unsaturated with gold and arsenopyrite with invisible gold was deposited. At the second productive stage of formation of gold-polysulfide mineralization, the fluid was saturated with gold and its nano and micro inclusions in arsenopyrite were formed. At the Olimpiada, gold is deposited on the surface of arsenopyrite crystals, indicating a later interaction of Au-containing fluid with previously formed arsenopyrite.

At the Bazovskoye deposit, a possible mechanism for the precipitation of dendrite-like gold in arsenopyrite replaced by scorodite may be the dissolution of arsenopyrite during interaction with Au-S(−As)-containing alkaline hydrothermal solutions in an oxidizing environment and its metasomatic replacement. The reaction of gold precipitation with scorodite is possible:

$$FeAsS(s.) + 2H_2O + 2.5O_2 + Au(HS)_2^- + 3OH^- = FeAsO_4 \cdot 2H_2O(s.) + Au(s.) + 2HS^- + SO_4^{2-}$$

Evidence of such a process is the residual fragments of arsenopyrite crystals and its intergrowths with native gold and scorodite. Gold is also characterized by increased solubility in alkaline sulfide solutions The dominant form of transport in alkaline solutions is the bisulfide complex of gold $Au(HS)_2^-$ (Benning and Seward, 1996; Stefansson and Seward, 2004; Pal'yanova, 2008; Williams-Jones et al., 2009).

The frequent association of arsenopyrite with pyrite-bearing sedimentary rocks, and numerous examples of the overgrowth of high-gold-bearing arsenopyrite on framboidal pyrite suggest the important role of syngenetic pyrite in the formation of gold-bearing arsenopyrite. One of the reasons for the enrichment of acicular arsenopyrite in gold is considered to be the high structural defect, which is determined by the ratio of Fe, As, and S in comparison with well-crystallized arsenopyrite (Zhmodik, 2008) explained by the lower temperature conditions of ore formation and later formation of gold in association with carbonates, sericite and chlorite. Inclusions, veinlets, and overgrowths of gold on corroded and deformed arsenopyrite crystals evidence this.

According to HRXCT studies of gold distribution in large crystals of arsenopyrite from ores of the Bazovskoe deposit it was found that gold shows selective crystallization not only within the aggregate of arsenopyrite crystals in the ore zone, but also among the crystallographic directions of a single arsenopyrite crystals. However, the question remains unanswered whether these crystallographic directions are planes in the areas of tension during deformation of arsenopyrite aggregates or planes most energetically favorable for gold crystallization.

Previous data for the Suzdal and other deposits in Eastern Kazakhstan (Kovalev et al., 2009, 2011, 2012; Rafailovich, 2009; Kalinin et al., 2019) are confirmed and supplemented by the results of this study. Acicular-prismatic arsenopyrite of the early productive stage is characterized by high gold content (1400–5360 g/t), high sulfur content S/As = 1.2 and is depleted in iron. According to the HRXCT 3D reconstruction established that within single grain and aggregates of arsenopyrite, gold is absent in the center (Fig. 3B) and is concentrated in the marginal parts of arsenopyrite crystals (Fig. 3D). This distribution of gold indicates the emergence of arsenopyrite nuclei and subsequent deposition of gold in the form of nanoscale particles coprecipitating together with arsenopyrite. Perhaps there was a pulsed supply of ore-bearing fluid at the first stage, and a local redistribution of Au at the second.

Tabular arsenopyrite in gold-polysulfide mineralization is characterized by lower gold content, elevated antimony concentrations and stoichiometric composition (Fig. 4). Visible gold is commonly superimposed on tabular arsenopyrite, indicating later gold deposition and apparently lower gold concentrations in the hydrothermal solution.

The ore formation at Suzdal deposit was long and can be divided into four stages. The first stage is associated with the accumulation of low gold-content pyrite, syngenetic to the ore-bearing strata. The second stage is associated with the formation of the first productive highly gold-bearing acicular arsenopyrite in the tectonic zone, with "invisible gold", accompanied by sericitization. In the third stage, silicified stockwork-type ores with nested-disseminated polymetallic mineralization and free visible gold were formed. The process ended with the formation of quartz-stibnite veins, superimposed on all previous types of ores. The time gap between the second and third productive stages, according to Ar/Ar dating of sericites, is 33 million years (Kovalev et al., 2012).

The main productive arsenopyrite mineralization at the Olympiada deposit was deposited at 689 ± 28 Ma (Re-Os), postdated by later berthierite-stibnite mineralization, deposited at 672.7 ± 4. 1 Ma (Ar-Ar). Main stage of mineralization correlate with intrusion of alkaline mafic rocks of the Zahrebetinskiy complex which was formed within the interval of 703–696 Ma (Ar-Ar). The age of antimony mineralization coincides with the age of the Chapinskiy alkaline picrite-carbonatite complex (670–650 Ma). Similar age for the gold-sulfide mineralization is established at other deposits of the Yenisei Ridge. The involvement of magmatic fluids from concurrent mafic alkaline, alkaline granite and granitoid melts in ore genesis is supported by fluid inclusion studies. The isotope-geochemical characteristics (Pb, Os, He, and S) of gold-arsenopyrite, gold-polysulfide, and stibnite-berthierite parageneses of ores at the Olympiada deposit suggest that different isotopic reservoirs could have served as the sources of ore material and fluids (Naumov et al., 2015).

Arsenopyrites of various structures and chemical compositions from early formed disseminated ores and late vein formations have been described also at the Natalka and Mayskoye deposits in northeastern Russia (Volkov et al., 2007). The presence of two morphological differences and compositions of arsenopyrite in single deposit allowed us to evaluate the duration of ore deposition processes and suggest the combination of different-stage of mineralization. The listed features indirectly indicate the possible high resources of gold at the studied deposit. As a rule, the multistage ore formation in such deposits is confirmed by other mineralogical evidence and isotope-geochronological data (Kovalev et al., 2009).

The use of HRXCT in the mineralogical study will allow at the early exploration stages to identify the above-described criteria to reduce costs and optimize the exploration process of the deposit.

6. Concluding remarks

Methods of high-resolution X-ray microtomography allow to reliably identify dense phases, such as inclusions of native gold in crystals of a mineral-concentrator (arsenopyrite, pyrite) without destroying the hosted mineral grains. But HRXCT study is most effective when it is used together with other methods such as optical microscopy, SEM, EMPA, LA-ICP-MS.

The results of studies of gold-bearing arsenopyrite from three typical orogenic gold deposits in NE Asia such as Suzdal (East Kazakhstan), Olympiada (Yenisei Ridge, Russia) and Bazovskoe (Yakutia, Russia), occurring mainly in black shales, two productive stages of ore deposition are distinguished, which correspond to two morphological varieties of arsenopyrite. At the early stage, fine-grained acicular-prismatic arsenopyrite with invisible gold was deposited; at the late stage, tabular arsenopyrite in association with free visible gold was formed.

Based on research performed, integrated with available publications, we can suggest that HRXCT technique permits.

(1) To do some estimation of the amount of gold inclusions in minerals or host rocks and draw reasonable conclusions about the gold content of the ores.

(2) To study in detail the distribution patterns of metal inclusions (associated with certain minerals, cracks, crystal growth faces, etc.) and to preliminarily evaluate the morphology of grains and veinlets without destroying the matrix.

(3) Applying complex methodologies (HRXCT combined with quantitative analysis of gold content) to determine the form of the metal; to define which type of gold makes the greatest contribution to the economic productivity of mineralization – the inclusion of native gold or ‘‘invisible” gold in the form of nanoparticles or structural impurities.

(4) HRXCT studies offer new opportunities for the development of efficient technologies for ore processing in order to maximize the extraction of the gold and silver.

CRediT authorship contribution statement

Evgeny Naumov: Writing – review & editing, Writing – original draft, Resources, Methodology, Investigation, Data curation, Conceptualization. **Yuri Kalinin:** Resources, Data curation, Conceptualization. **Galina Palyanova:** Writing – review & editing, Formal analysis, Conceptualization. **Lyudmila Kryuchkova:** Visualization, Methodology, Investigation. **Viacheslav Voitenko:** Methodology, Investigation. **Vera Abramova:** Visualization, Methodology, Investigation. **Franco Pirajno:** Writing – review & editing, Methodology, Conceptualization.

Declaration of competing interest

The authors declare that they have no known competing financial interests or personal relationships that could have appeared to influence the work reported in this paper.

Acknowledgements

This paper is to the treasured memory of Konstantin Kovalev, an outstanding geologistand researcher who devoted many years to studying the ore deposits. The HRCT studies of the samples were carried out jointly with colleagues within the framework of the Research Agreement with the Saint Petersburg State University No C-103/11 signed 08.09.2017. We are grateful to them for their cooperation. We thank the anonymous reviewers and editors for their comments and suggestions, which helped to improve the manuscript. The work was carried out with financial support for the project by the Russian Federation represented by the Ministry of Education and Science of Russia (project number 13.1902.24.44, agreement number 075-15-2024-641).

References

Agorhom, E.A., Skinner, W., Zanin, M., 2012. Upgrading of low-grade gold ore samples for improved particle characterisation using Micro-CT and SEM/EDX. Adv. Powder Technol. 23, 498–508. https://doi.org/10.1016/j.apt.2012.04.011.

Arehart, G.B., Chryssoulis, S.L., Kesler, S.E., 1993. Gold and arsenic in iron sulfides from sediment-hosted disseminated gold deposits; implications for depositional processes. Econ. Geol. 88, 171–185. https://doi.org/10.2113/gsecongeo.88.1.171.

Barnes, S.J., Fiorentini, M.L., Austin, P., Gessner, K., Hough, R.M., Squelch, A.P., 2008. Three-dimensional morphology of magmatic sulfides sheds light on ore formation and sulfide melt migration. Geology 36, 655. https://doi.org/10.1130/G24779A.1.

Benning, L.G., Seward, T.M., 1996. Hydrosulfide complexing of Au (I) in hydrothermal solutions from 150–400 °C and 500–1500 bars. Geochim. Cosmochim. Acta 60, 1849–1872.

Benzaazoua, M., Marion, P., Robaut, F., Pinto, A., 2007. Gold-bearing arsenopyrite and pyrite in refractory ores: analytical refinements and new understanding of gold mineralogy. Mineral. Mag. 71, 123–142.

Bindi, L., Moelo, Y., Leone, P., Suchaud, M., 2012. Stoichiometric arsenopyrite, FeAsS, from La Roche-Balue Quarry, Loire-Atlantique, France: crystal structure and Mössbauer study. Can. Miner. 50, 471–479. https://doi.org/10.3749/canmin.50.2.471.

Cabri, L.J., Newville, M., Gordon, R.A., Crozier, E.D., Sutton, S.R., McMahon, G., Jiang, D.-T., 2000. Chemical speciation of gold in arsenopyrite. Can. Miner. 38, 1265–1281. https://doi.org/10.2113/gscanmin.38.5.1265.

Cathelineau, M., Boiron, M.C., Holliger, P., Marion, P., Denis, M., 1989. Gold in arsenopyrites: crystal chemistry, location and state, physical chemical conditions of deposition. The geology of Gold deposits: The Perspective in 1988. Econ. Geol. Monograph 6, 328–340.

Chetty, D., Clark, W., Bushell, C., Sebola, T.P., Hoffman, J., Nshimirimana, R., De Beer, F., 2012. In: The Use of 3D X-Ray Computed Tomography for Gold Location in Exploration Drill Cores. Springer Berlin Heidelberg, Berlin, Heidelberg, pp. 129–136. https://doi.org/10.1007/978-3-642-27682-8_17.

Chisambi, J., von der Heyden, B., Tshibalanganda, M., Le Roux, S., 2020. Gold exploration in two and three dimensions: improved and correlative insights from microscopy and X-Ray computed tomography. Minerals 10, 476. https://doi.org/10.3390/min10050476.

Cnudde, V., Boone, M.N., 2013. High-resolution X-ray computed tomography in geosciences: a review of the current technology and applications. Earth-Sci. Rev. 123, 1–17. https://doi.org/10.1016/j.earscirev.2013.04.003.

Cook, N.J., Ciobanu, C.L., Meria, D., Silcock, D., Wade, B., 2013. Arsenopyrite-pyrite association in an orogenic gold ore: tracing mineralization history from textures and trace elements. Econ. Geol. 108, 1273–1283. https://doi.org/10.2113/econgeo.108.6.1273.

da Costa, M.F., Kyle, J.R., Lobato, L.M., Ketcham, R.A., Figueiredo, R.C., Silva, F., Fernandes, R.C., 2022. Orogenic gold ores in three-dimensions: a case study of distinct mineralization styles at the world-class Cuiabá deposit, Brazil, using high-resolution X-ray computed tomography on gold particles. Ore Geol. Rev. 140, 104584.

Deditius, A.P., Reich, M., Kesler, S.E., Utsunomiya, S., Chryssoulis, S.L., Walshe, J., Ewing, R.C., 2014. The coupled geochemistry of Au and As in pyrite from hydrothermal ore deposit. Geochim. Cosmochim. Acta 140, 644–670.

Fatima, A., Venkatesh, A.S., Mukherjee, R., Agrawal, A.K., Singh, B., Sarkar, P.S., Shripathi, T., 2019. 3D spatial distribution of ore mineral phases using high resolution synchrotron micro-computed tomography (μCT) combined with optical microscopy. Appl. Radiat. Isot. 148, 49–59.

Fougerouse, D., Reddy, S.M., Saxey, D.W., Rickard, W.D.A., van Riessen, A., Micklethwaite, S., 2016. Nanoscale gold clusters in arsenopyrite controlled by growth rate not concentration: evidence from atom probe microscopy. Am. Miner. 101, 1916–1919. https://doi.org/10.2138/am-2016-5781CCBYNCND.

Fridovsky, V.Y., Gamyanin, G.N., Polufuntikova, L.I., 2015. Structures, mineralogy, and fluid regime of ore formation in the polygenetic Malo-Taryn gold field, Northeast Russia. Rus. J. Pacific Geol. 9, 274–286. https://doi.org/10.1134/S1819714015040028.

Fridovsky, V.Y., Polufuntikova, L.I., Goryachev, N.A., Kudrin, M.V., 2017. Ore-controlling thrust faults at the Bazovskoe gold-ore deposit (Eastern Yakutia). Doklady Earth Sci. 474, 617–619. https://doi.org/10.1134/S1028334X17060034.

Fridovsky, V.Y., Polufuntikova, L.I., Kudrin, M.V., 2023. Origin of disseminated gold-sulfide mineralization from proximal alteration in orogenic gold deposits in the central sector of the Yana-Kolyma Metallogenic Belt, NE Russian. Minerals 13, 394. https://doi.org/10.3390/min13030394.

Genkin, A.D., Bortnikov, N.S., Cabri, L.J., Wagner, F.E., Stanley, C.J., Safonov, Y.G., McMahon, G., Friedl, J., Kerzin, A.L., Gamyanin, G.N., 1998. A multidisciplinary study of invisible gold in arsenopyrite from four mesothermal gold deposits in Siberia, Russian Federation. Econ. Geol. 93, 463–487. https://doi.org/10.2113/gsecongeo.93.4.463.

Ghorbani, Y., Becker, M., Petersen, J., Morar, S.H., Mainza, A., Franzidis, J.-P., 2011. Use of X-ray computed tomography to investigate crack distribution and mineral dissemination in sphalerite ore particles. Minerals Eng. 24, 1249–1257. https://doi.org/10.1016/j.mineng.2011.04.008.

Godel, B., 2013. High-resolution X-Ray computed tomography and its application to ore deposits: from data acquisition to quantitative three-dimensional measurements with case studies from Ni-Cu-PGE deposits. Econ. Geol. 108, 2005–2019. https://doi.org/10.2113/econgeo.108.8.2005.

Goldfarb, R.J., Baker, T., Dube, B., Groves, D.I., Hart, C.J.R., Gosselin, P., 2005. Distribution, character, and genesis of gold deposits in metamorphic terranes. Society of Economic Geologists, Littleton, Colorado, pp. 407–450.

Goldfarb, R.J., Pitcairn, I., 2023. Orogenic gold: is a genetic association with magmatism realistic? Mineral. Deposit. 58 (1), 5–35. https://doi.org/10.1007/s00126-022-01146-8.

Groves, D.I., Goldfarb, R.J., Gebre-Mariam, M., Hagemann, S.G., Robert, F., 1998. Orogenic gold deposits: a proposed classification in the context of their crustal distribution and relationship to other gold deposit types. Ore Geol. Rev. 13 (1), 7–27.

Groves, D.I., Santosh, M., Deng, J., Wang, Q., Yang, L., Zhang, L., 2020. A holistic model for the origin of orogenic gold deposits and its implications for exploration. Mineral. Deposit. 55 (2), 275–292. https://doi.org/10.1007/s00126-019-00877-5.

Guntoro, P.I., Ghorbani, Y., Koch, P.-H., Rosenkranz, J., 2019. X-ray microcomputed tomography (μCT) for mineral characterization: a review of data analysis methods. Minerals 9, 183. https://doi.org/10.3390/min9030183.

Hayashi, K.I., Ohmoto, H., 1991. Solubility of gold in NaCl and H_2S bearing aqueous solutions at 250–350 ℃. Geochim. Cosmochim. Acta 55, 2111–2126.

Hinchey, J.G., Wilton, D.H.C., Tubrett, M.N., 2003. A LAM ICP MS study of the distribution of gold in arsenopyrite from the Lodestar prospect, Newfoundland, Canada. Can. Mineral. 41, 353–364. https://doi.org/10.2113/gscanmin.41.2.353.

Hough, R.M., Noble, R.R.P., Reich, M., 2011. Natural gold nanoparticles. Ore Geol. Rev. 42, 55–61. https://doi.org/10.1016/j.oregeorev.2011.07.003.

Jelic, I., Zavasnik, J., Lazarov, M., Zdravkovic, A., Kovac, S., Stojanovic, J., Pacevski, A., 2023. Micro- to nanoscale textures of gold in arsenopyrite and scorodite from the As-Au-Bi assemblage of Drenjak locality (Serbia). Ore Geol. Rev. 163, 105711. https://doi.org/10.1016/j.oregeorev.2023.105711.

Jiang, S.-Y., Ma, Y., Liu, D.-L., Li, W.-T., 2023. Orogenic gold deposits: mineralization mechanism and research perspectives. J. Earth Sci. 34 (6), 1758–1761. https://doi.org/10.1007/s12583-023-2005-1.

Kalinin, Y.A., Naumov, E.A., Borisenko, A.S., Kovalev, K.R., Antropova, A.I., 2015. Spatial-temporal and genetic relationships between gold and antimony mineralization at gold-sulfide deposits of the Ob-Zaisan folded zone. Geol. Ore Deposit. 57, 157–171. https://doi.org/10.1134/S1075701515030022.

Kalinin, Y.A., Palyanova, G.A., Naumov, E.A., Kovalev, K.R., Pirajno, F., 2019. Supergene remobilization of Au in Au-bearing regolith related to orogenic deposits: a case study from Kazakhstan. Ore Geol. Rev. 109, 358–369. https://doi.org/10.1016/j.oregeorev.2019.04.019.

Ketcham, R.A., 2005. Computational methods for quantitative analysis of three-dimensional features in geological specimens. Geosphere 1, 32. https://doi.org/10.1130/GES00001.1.

Khishgee, C., Akasaka, M., 2015. Mineralogy of the Boroo Gold Deposit in the North Khentei Gold Belt, Central Northern Mongolia. Res. Geol. 65 (4), 311–327. https://doi.org/10.1111/rge.12073.

Kovalchuk, E.V., Tagirov, B.R., Vikentyev, I.V., Chareev, D.A., Tyukova, E.E., Nikolsky, M.S., Bortnikov, N.S., 2019. "Invisible" gold in synthetic and natural arsenopyrite crystals, Vorontsovka Deposit, Northern Urals. Geol. Ore Deposit. 61, 447–468. https://doi.org/10.1134/S1075701519050039.

Kovalev, K.R., Kalinin, Y.A., Naumov, E.A., Pirajno, F., Borisenko, A.S., 2009. A mineralogical study of the Suzdal sediment-hosted gold deposit, Eastern Kazakhstan: implications for ore genesis. Ore Geol. Rev. 35, 186–205. https://doi.org/10.1016/j.oregeorev.2008.11.007.

Kovalev, K.R., Kalinin, Y.A., Naumov, E.A., Kolesnikova, M.K., Korolyuk, V.N., 2011. Gold-bearing arsenopyrite in eastern Kazakhstan gold-sulfide deposits. Rus. Geol. Geophy. 52, 178–192. https://doi.org/10.1016/j.rgg.2010.12.014.

Kovalev, K.R., Kalinin, Y.A., Polynov, V.I., Kydyrbekov, E.L., Borisenko, A.S., Naumov, E.A., Netesov, M.I., Klimenko, A.G., Kolesnikova, M.K., 2012. The Suzdal gold-sulfide deposit in the black shale of Eastern Kazakhstan. Geol. Ore Deposit. 54, 254–275. https://doi.org/10.1134/S1075701512040034.

Kravtsova, R.G., Tauson, V.L., Nikitenko, E.M., 2015. Modes of Au, Pt, And Pd occurrence in arsenopyrite from the Natalkinskoe deposit, NE Russia. Geochem. Int. 53 (11), 964–972. https://doi.org/10.1134/S0016702915090037.

Kudrin, M.V., Fridovsky, V.Y., Polufuntikova, L.I., Kryuchkova, L.Y., 2021. Disseminated gold-sulfide mineralization in metasomatites of the Khangalas Deposit, Yana-Kolyma Metallogenic belt (Northeast Russia): analysis of the texture, geochemistry, and S isotopic composition of pyrite and arsenopyrite. Minerals 11, 403. https://doi.org/10.3390/min11040403.

Kyle, J.R., Ketcham, R.A., 2015. Application of high resolution X-ray computed tomography to mineral deposit origin, evaluation, and processing. Ore Geol. Rev. 65, 821–839. https://doi.org/10.1016/j.oregeorev.2014.09.034.

Kyle, J.R., Mote, A.S., Ketcham, R.A., 2008. High resolution X-ray computed tomography studies of Grasberg porphyry Cu-Au ores, Papua, Indonesia. Miner. Deposit. 43, 519–532. https://doi.org/10.1007/s00126-008-0180-8.

Liang, Y., Ge, H., Pei, Q., Huang, H., Hoshino, K., 2023. 3D plotting of gold solubility and gold fineness: quantitative analysis of ore-forming conditions in hydrothermal gold deposits. Lithosphere 208, 21. https://doi.org/10.2113/2023/lithosphere_2023_208.

Lohmeier, S., Gainov, R.R., Hodgkin, A., 2023. Morphological characterization of lode gold in the auriferous quartz veins at M'Popo mine, Angola, by computed tomography and optical microscopy. Appl. Earth Sci. 132 (2), 1–25. https://doi.org/10.1080/25726838.2023.2219116.

Merkulova, M., Mathon, O., Glatzel, P., Rovezzi, M., Batanova, V., Marion, P., Boiron, M.-C., Manceau, A., 2019. Revealing the chemical form of "invisible" gold in natural arsenian pyrite and arsenopyrite with high energy-resolution X-ray absorption spectroscopy. ACS Earth Space Chem. 3, 1905–1914. https://doi.org/10.1021/acsearthspacechem.9b00099.

Morey, A.A., Tomkins, A.G., Bierlein, F.P., Weinberg, R.F., Davidson, G.J., 2008. Bimodal distribution of gold in pyrite and arsenopyrite: examples from the Archean Boorara and bardoc shear systems, Yilgarn Craton, Western Australia. Econ. Geol. 103, 599–614. https://doi.org/10.2113/gsecongeo.103.3.599.

Naumov, E.A., Borisenko, A.S., Nevolko, P.A., Kovalev, K.R., Tessalina, S., Sazonov, A. M., Savichev, A.A., Zvyagina, E.A., 2015. Gold-sulfide (Au-As) Deposits of the Yenisei Ridge (Russia): age, sources of metals and nature of fluids. Min. Resour. Sustain. World 1–5, 165–168.

Naumov, E., Kovalev, K., Kalinin, Yu., Palyanova, G., Voitenko, V., 2019. High resolution 3D x-ray computed tomography: Application for the study of gold-bearing arsenopyrite. Life with ore deposits on Earth. Proceedings of the 15th SGA Biennial Meeting 2, 803–806.

Nozhkin, A.D., Borisenko, A.S., Nevol'ko, P.A., 2011. Stages of Late Proterozoic magmatism and periods of Au mineralization in the Yenisei Ridge. Rus. Geol. Geophys. 52, 124–143. https://doi.org/10.1016/j.rgg.2010.12.010.

Pal'yanova, G., 2008. Physicochemical modeling of the coupled behavior of gold and silver in hydrothermal processes: gold fineness, Au/Ag ratios and their possible implications. Chem. Geol. 255, 399–413. https://doi.org/10.1016/j.chemgeo.2008.07.010.

Palenik, C.S., Utsunomiya, S., Reich, M., Kesler, S.E., Wang, L., Ewing, R.C., 2004. "Invisible" gold revealed: direct imaging of gold nanoparticles in a Carlin-type deposit. Am. Miner. 89, 1359–1366. https://doi.org/10.2138/am-2004-1002.

Phillips, G.N., Powell, R., 2010. Formation of gold deposits: a metamorphic devolatilization model. J. Metamorphic Geol. 28 (6), 689–718. https://doi.org/10.1111/j.1525-1314.2010.00887.x.

Phillips, G.N., 2013. Australian and global setting for gold in 2013, in Proceedings World Gold 2013, Brisbane, Australia, 26–29 September, 2013. The Australian Institute of Mining and Metallurgy, p. 15–21.

Rafailovich, M.S., 2009. Gold Deposits of Kazakhstan: Geology, Metallogeny, Exploration Models. Almaty, Kazakhstan.

Safonova, I., Kotlyarov, A., Krivonogov, S., Xiao, W., 2017. Intra-oceanic arcs of the Paleo-Asian Ocean. Gondwana Res. 50, 167–194. https://doi.org/10.1016/j.gr.2017.04.005.

Sazonov, A.M., Lobanov, K.V., Zvyagina, E.A., Leontiev, S.I., Silyanov, S.A., Nekrasova, N.A., Borodushkin, A.B., Poperekov, V.A., Zhuravlev, V.V., Ilyin, S.S., Kalinin, Yu.A., Savichev, A.A., Yakubchuk, A.S., 2020. Olympiada Gold Deposit, Yenisei Ridge, Russia. Society of Economic Geologists, Inc. SEG Special Publications 23, 203–226. https://doi.org/10.5382/SP.23.10.

Sazonov, A.M., Kirik, S.D., Silyanov, S.A., Bayukov, O.A., Tishin, P.A., 2016. Typomorphism of arsenopyrite from the Blagodatnoe and Olimpiada gold deposits (Yenisei Ridge). Mineralogy 3, 53–70.

Sazonov, A.M., Silyanov, S.A., Bayukov, O.A., Knyazev, Y.V., Zvyagina, Y.A., Tishin, P. A., 2019a. Composition and ligand microstructure of arsenopyrite from gold ore deposits of the Yenisei Ridge (Eastern Siberia, Russia). Minerals 9, 737. https://doi.org/10.3390/min9120737.

Sazonov, A.M., Zvyagina, E.A., Silyanov, S.A., Lobanov, K.V., Leontyev, S.I., Kalinin, Y. A., Savichev, A.A., Tishin, P.A., 2019b. Ore genesis of the Olimpiada gold deposit (Yenisei Ridge, Russia). Geosphere Res., 17–43 https://doi.org/10.17223/25421379/10/2.

Sidorova, N.V., Aristov, V.V., Grigor'eva, A.V., Sidorov, A.A., 2020. "Invisible" gold in pyrite and arsenopyrite from the Pavlik deposit (northeastern Russia). Doklady Earth Sci. 495 (1), 821–826.

Silyanov, S.A., Sazonov, A.M., Naumov, E.A., Lobastov, B.M., Zvyagina, Y.A., Artemyev, D.A., Nekrasova, N.A., Pirajno, F., 2022. Mineral Paragenesis, formation stages and trace elements in sulfides of the Olympiada gold deposit (Yenisei Ridge, Russia). Ore Geol. Rev. 143, 104750. https://doi.org/10.1016/j.oregeorev.2022.104750.

Stefansson, A., Seward, T.M., 2004. Gold (I) complexing in aqueous sulphide solutions to 500 °C at 500 bar. Geochim. Cosmochim. Acta 68, 4121–4143.

Sung, Y.H., Brugger, J., Ciobanu, C.L., Pring, A., Skinner, W., Nugus, M., 2009. Invisible gold in arsenian pyrite and arsenopyrite from a multistage Archaean gold deposit: sunrise Dam, Eastern Goldfields Province, Western Australia. Miner. Depos. 44, 765. https://doi.org/10.1007/s00126-009-0244-4.

Tauson, V.L., Kravtsova, R.G., Smagunov, N.V., 2014. Structural and surface–bond gold in pyrite from deposits of various genetic types. Russ. Geol. Geophys. 55, 350–369.

Tauson, V., Lipko, S., Kravtsova, R., Smagunov, N., Belozerova, O., Voronova, I., 2019. Distribution of "invisible" noble metals between pyrite and arsenopyrite exemplified by minerals coexisting in orogenic Au deposits of North-Eastern Russia. Minerals 9, 660. https://doi.org/10.3390/min9110660.

Trigub, A.L., Tagirov, B.R., Kvashnina, K.O., Chareev, A., Nickolsky, M.S., Shiryaev, A. A., Baranova, N.N., Kovalchuk, E.V., Mokhov, A.V., 2017. X-ray spectroscopy study of the chemical state of "invisible" Au in synthetic minerals in the Fe-As-S system. Am. Miner. 102, 1057–1065. https://doi.org/10.2138/am-2017-5832.

Vikentyev, I., Vikent'eva, O., Tyukova, E., Nikolsky, M., Ivanova, J., Sidorova, N., Tonkacheev, D., Abramova, V., Blokov, V., Spirina, A., Borisova, D., Palyanova, G., 2021. Noble metal speciations in hydrothermal sulphides. Minerals 11, 488. https://doi.org/10.3390/min11050488x.

Voitenko, V.N., 2014. Native gold crystallization form in arsenopyrite's ore from Bazovsky deposite (from X-Ray Tomography data). Proceedings of the III Conf. "Practical Microtomography", St. Petersburg 26–28.

Volkov, A.V., Genkin, A.D., Goncharov, V.I., 2007. Gold species in ores of the Natalkinskoe and Maiskoe deposits (northeastern Russia). Tikhookeanskaya Geologiya 25, 18–29.

Warlo, M., Bark, G., Wanhainen, C., Butcher, A.R., Forsberg, F., Lycksam, H., Kuva, J., 2021. Multi-scale X-ray computed tomography analysis to aid automated mineralogy in ore geology research. Front. Earth Sci. 9, 789372. https://doi.org/10.3389/feart.2021.789372.

Williams-Jones, A.E., Bowell, R.J., Migdisov, A.A., 2009. Gold in solution. Elements 5 (5), 281–287. https://doi.org/10.2113/gselements.5.5.281.

Zhmodik, S.M., 2008. Gold-Concentrating Systems of Ophiolite Belts (by the Example of the Sayan–Baikal–Muya Belt). Akademicheskoe Izd. "Geo", Novosibirsk (in Russian).